HHS Public Access

Author manuscript

Matrix Biol. Author manuscript; available in PMC 2023 April 03.

Published in final edited form as:

Matrix Biol. 2022 August ; 111: 108–132. doi:10.1016/j.matbio.2022.06.004.

Matrix-bound Cyr61/CCN1 is required to retain the properties of the bone marrow mesenchymal stem cell niche but is depleted with aging

Milos Marinkovic[a,b,f], **Qiuxia Dai**[a], **Aaron O. Gonzalez**[a,b], **Olivia N. Tran**[a,b], **Travis J. Block**[a,b], **Stephen E. Harris**[c], **Adam B. Salmon**[d,e], **Chih-Ko Yeh**[a,e], **David D. Dean**[a,b], **Xiao-Dong Chen**[a,b,f]

[a] -**Department of Comprehensive Dentistry**, University of Texas Health Science Center at San Antonio, 7703 Floyd Curl Drive, San Antonio, TX 78229, United States

[b] -**Department of Biomedical Engineering**, University of Texas at San Antonio, San Antonio, TX 78249, United States

[c] -**Department of Periodontics**, University of Texas Health Science Center at San Antonio, TX 78229, United States

[d] -**Department of Molecular Medicine**, Barshop Institute for Longevity and Aging Studies at The University of Texas Health Science Center at San Antonio, San Antonio, TX 78229, United States

[e] -**Geriatric Research, Education and Clinical Center, South Texas Veterans Health Care System, Audie Murphy VA Medical Center**, San Antonio, TX 78229, United States

[f] -**Research Service, South Texas Veterans Health Care System**, Audie Murphy VA Medical Center, San Antonio, TX 78229, United States

Abstract

Previously, we showed that extracellular matrices (ECMs), produced *ex vivo* by various types of stromal cells, direct bone marrow mesenchymal stem cells (BM-MSCs) in a tissue-specific manner and recapitulate physiologic changes characteristic of the aging microenvironment. In particular, BM-MSCs obtained from elderly donors and cultured on ECM produced by young BM stromal cells showed improved quantity, quality and osteogenic differentiation. In the present study, we searched for matrix components that are required for a functional BM-MSC niche by comparing ECMs produced by BM stromal cells from “young” (≤25 y/o) versus “elderly” (≥60 y/o) donors.

Corresponding author at: Department of Comprehensive Dentistry, University of Texas Health Science Center at San Antonio, 7703 Floyd Curl Drive, San Antonio, TX 78229, United States. chenx4@uthscsa.edu.

Contributions

MM: designed and performed experiments, analyzed data, prepared figures/tables, prepared first draft of the manuscript; QD, AOG, ONT and TJB: performed experiments, acquired data; SEH and CKY: performed experiments, advised on data analysis and interpretation, wrote/edited manuscript; ABS: advised on aging mice and provided assistance with data analysis and interpretation; DDD: performed data analysis and interpretation, wrote/edited manuscript; XDC: conceived/designed the study, obtained financial support, analyzed/interpreted the data, wrote/edited manuscript; All authors have reviewed and approved the final manuscript.

Declaration of Competing Interest

Dr. Chen is a Board member and shareholder in StemBioSys, Inc. (San Antonio, TX). Dr. Travis Block is currently an employee of StemBioSys, Inc. (San Antonio, TX) and receives a salary. All other authors have no financial or competing interests to declare.

With increasing donor age, ECM fibrillar organization and mechanical integrity deteriorated, along with the ability to promote BM-MSC proliferation and responsiveness to growth factors. Proteomic analyses revealed that the matricellular protein, Cyr61/CCN1, was present in young, but undetectable in elderly, BM-ECM. To assess the role of Cyr61 in the BM-MSC niche, we used genetic methods to down-regulate the incorporation of Cyr61 during production of young ECM and up-regulate its incorporation in elderly ECM. The results showed that Cyr61-depleted young ECM lost the ability to promote BM-MSC proliferation and growth factor responsiveness. However, up-regulating the incorporation of Cyr61 during synthesis of elderly ECM restored its ability to support BM-MSC responsiveness to osteogenic factors such as BMP-2 and IGF-1. We next examined aging bone and compared bone mineral density and Cyr61 content of L4-L5 vertebral bodies in “young” (9–11 m/o) and “elderly” (21–33 m/o) mice. Our analyses showed that low bone mineral density was associated with decreased amounts of Cyr61 in osseous tissue of elderly versus young mice. Our results strongly demonstrate a novel role for ECM-bound Cyr61 in the BM-MSC niche, where it is responsible for retention of BM-MSC proliferation and growth factor responsiveness, while depletion of Cyr61 from the BM niche contributes to an aging-related dysregulation of BM-MSCs. Our results also suggest new potential therapeutic targets for treating age-related bone loss by restoring specific ECM components to the stem cell niche.

Keywords

Stem cell niche; Aging; Extracellular matrix; Cyr61/CCN1; Bone microenvironment; Osteogenic differentiation

Introduction

The activity of mesenchymal stem cells (MSCs) *in vivo* is orchestrated by the local tissue-specific microenvironment or niche, which not only regulates MSC self-renewal, preventing mitotic exhaustion or neoplasia of these cell reservoirs, but also directs differentiation for tissue repair and maintenance of homeostasis [1–3]. The MSC niche for each tissue consists of a unique collection of extracellular matrix (ECM) proteins, organized as a three-dimensional (3D) microenvironment, to provide the appropriate chemical, mechanical, and physical cues, or “tissue-specific” instructions, for the resident cells. During aging, MSCs lose their ability to self-renew and differentiate and contain increased numbers of senescent cells, which negatively impact their ability to maintain tissue homeostasis [4–7]. A comprehensive understanding of the dynamic reciprocity between MSCs and their ECM, as well as how alterations in ECM properties during aging impair MSC function, requires a culture system that closely replicates the *in vivo* MSC microenvironment.

Our group was the first to describe the preparation of a native 3D-ECM culture system that faithfully reproduced the stem cell niche using bone marrow (BM)-derived stromal cells from both mice and humans [8,9]. By use of this culture system, we were able to demonstrate that the ECM promoted BM-MSC attachment, proliferation, and motility (directional movement and reduced cell-to-cell contact) and retained the differentiation capacity of the cells relative to ordinary (2D) tissue culture plastic (TCP) [10,11]. Further, bone formation capacity of elderly murine BM-MSCs could be restored by culture on

ECM synthesized by young stromal cells. In contrast, ECM synthesized by elderly stromal cells failed to promote BM-MSC self-renewal and differentiation capacity (e.g. ability to form bone) was remarkably diminished [12]. Taken together, the above observations firmly established that tissue-specific ECM-based culture systems provide a method for identifying and studying key ECM components that control BM-MSC fate [13,14].

In the present report, we used mass spectrometry to identify age-related changes in the proteome of ECM produced by human BM stromal cells from "young" (≤25-year old) versus "elderly" (≥60-year old) donors. The results showed that cysteine-rich angiogenic inducer 61 (Cyr61) was abundant in young ECM but absent in elderly ECM.

Cyr61, also known as CCN1, is a member of the CCN (Cellular Communication Network) family of matricellular proteins that coordinate signaling among ECM secreted proteins and cell surface receptors [15–17]. Unlike structural ECM proteins, matricellular proteins primarily play a local regulatory role and direct cell function/activity by binding to membrane receptors and/or serving as cofactors in signal transduction pathways [17–19]. CCN proteins contain four binding domains which interact with growth factors such as IGF-1 and members of the TGF-β superfamily (e.g. BMP-2) [19,20]. Cyr61 regulates an array of cellular activities including: survival [21–24]; embryonic development [25–27], wound healing [28–32], tumorigenesis [33–39], senescence [40,41], and stem/progenitor cell-mediated tissue homeostasis (e.g. angiogenic, myogenic and osteogenic differentiation) [42–50]. Recently, Zhao et al. employed a transgenic mouse model to show that bone-specific knockout of Cyr61 resulted in the attenuation of osteoblast and osteocyte function and reduced bone mass relative to the wild-type [51] While it has been demonstrated that intracellular Cyr61 regulates the activity of stem/progenitor cells, its principal role as an extracellular protein (i.e. as a signaling cue within the ECM) remains largely undefined. This is due to the absence of an appropriate *in vitro* model for studying the BM-MSC niche in general and Cyr61 within the context of the ECM in particular.

Based on these observations, we hypothesized that loss of matrix-bound Cyr61 during aging negatively impacts the BM-MSC niche and contributes to the loss of BM-MSC properties. To test this hypothesis, we studied the behavior of BM-MSCs cultured on cell-derived ECMs, modified by genetic methods to either down-regulate (knockdown) or up-regulate the incorporation of Cyr61 protein in young ECM (yECM) and elderly ECM (eECM), respectively.

Results

BM-MSCs lose their stem cell properties when maintained on ECM produced by stromal cells from elderly donors. yECM and eECM were prepared using BM-derived stromal cells from young (≤25 years old) and elderly (≥60 years old) human donors. To compare the capacity of the two ECMs to support proliferation, young BM-MSCs were cultured on TCP, yECM or eECM for 5 days and the number of cells at the end of culture was determined (Fig. 1A). Only culture on yECM significantly promoted cell proliferation relative to TCP, while proliferation on eECM was significantly less than on yECM.

To examine the effect of culture substrate on differentiation, BM-MSCs were seeded onto TCP, yECM, or eECM and then cultured for 7 days in standard growth media. On day 7, the standard growth media were changed to low serum-containing media for 24 h, followed by adding either BMP-2 or rosiglitazone (Rgz) to the media for an additional 48 h to induce osteoblastogenesis or adipogenesis, respectively.

BM-MSCs cultured on yECM displayed the most robust response to BMP-2 (200 ng/ml) with a 1.9-fold increase in the expression of runt-related transcription factor 2 (Runx2, an osteoblast-specific transcription factor) as compared to untreated controls (Fig. 1B). In contrast, BM-MSCs cultured on eECM or TCP did not show any significant increase in Runx2 expression with BMP-2 treatment. When expression of bone sialoprotein (BSP, an osteoblast marker) was measured after growth factor treatment (Fig. 1C), BM-MSCs cultured on yECM showed a 2.6-fold increase in response, which was similar to that observed for Runx2. Cells on eECM demonstrated a lower level of response at 1.5-fold, while those on TCP showed no significant response.

In parallel studies, cells cultured on the various substrates and treated with Rgz to induce adipogenesis showed an opposite trend. The only significant fold-increase in peroxisome proliferator-activated receptor gamma (PPARγ, an adipocyte-specific transcription factor) expression was found in BM-MSCs cultured on eECMs (1.4-fold) (Fig. 1D).

Young and elderly ECMs display substantial differences in architecture, mechanical properties and protein composition

Atomic force microscopy (AFM) was used to characterize the architectural features of yECM and eECM (Fig. 2A). yECM was found to contain thin fibrillar structures that were more uniformly organized than those in eECM, which appeared thicker and irregularly organized. yECM contained fibers that were highly aligned (60–120°), indicating a narrow range of fiber orientations. In contrast, fibers in the eECM displayed a wider range of orientations (5–180°) (Fig. 2B). Topographic mapping was used to compute mean surface roughness (R_a) which showed that the surface of yECM was rougher than that of eECM (Fig. 2C). Stiffness of the ECMs was measured employing small angle oscillatory shear (SAOS) rheology; the storage modulus of yECM was almost 3X greater than that of eECM (Fig. 2D).

Proteomic analysis showed that yECM and eECM ($N = 4$ for each) shared a considerable number of protein components, constituting about 73% (19 out of 26) of the proteins found in yECM and approximately 43% (19 out of 44) of those identified in eECM (Fig. 3A). Overall, the largest proportion of shared ECM components was dominated by structural proteins, such as fibronectin, collagens (types I, III, V, VI and XII) and small proteoglycans (Fig. 3B). Although type I collagen was found in both ECMs, it was about 2-fold higher in yECM than eECM. There were 25 proteins identified solely in the eECM and the majority of these were glycoproteins and small proteoglycans (Fig. 3C). Interestingly, several proteins identified solely in eECM are negative regulators of collagen matrix deposition (e.g. CTHRC1, collagen triple helix repeat containing-1) or involved in matrix degradation (e.g. MMP-2, matrix metalloproteinase-2). The number of unique protein components in yECM was much smaller than that of eECM and included a single collagen

(type XI) (Fig. 3D). Importantly, the two most abundant proteins identified exclusively in yECM were CCN-family members: Cyr61 (CCN1) and CTGF (CCN2).

Production of Cyr61 and its incorporation into the ECM are decreased with aging

To validate the results of the proteomic analyses showing that Cyr61 was enriched in young- versus elderly-ECM, protein extracts of BM stromal cells and decellularized matrices from three young (<25y/o) and four elderly (>60y/o) donors were prepared for Western blot analysis (Fig. 4). Immunoblots of young BM-MSCs contained strong immunoreactive bands consistent with the molecular weight of Cyr61 (M_r 42–53 kDa), while blots of elderly cells showed little or no Cyr61 immunoreactivity (Fig. 4A). Mean Cyr61/GAPDH band intensities further confirmed that young BM stromal cells produced significantly higher amounts of Cyr61 than elderly cells (Fig. 4A, lower panel).

In parallel experiments, the abundance of matrix-bound Cyr61 in decellularized ECMs was compared using Western blot analysis. Consistent with the results of the cell lysate studies, all three immunoblots of the yECM protein lysates stained strongly for Cyr61, while those of the eECM stained weakly or not at all (Fig. 4B). Relatively weak staining for GAPDH suggested that contamination of the ECM lysates with cellular proteins was low. Quantitation of mean Cyr61 Western blot band density showed a statistically significant trend between intracellular expression of Cyr61 and its incorporation in the ECM by young and elderly BM stromal cells (Fig. 4B, lower panel). To further confirm the Western blot data, immunofluorescence microscopy of the ECMs was also performed (Fig. 4C). The results identified strong staining for Cyr61 in histologic sections of the young, but not elderly, ECMs. Taken together, these immunoblot and immunofluorescence studies, along with the proteomic profiling, indicate that matricellular Cyr61 is depleted in the eECM due to reduced production of Cyr61 by cells from the elderly donors.

Addition of exogenous Cyr61 is not as effective as yECM in promoting BM-MSC proliferation and BMP-2 responsiveness

To determine if exogenous Cyr61 promoted BM-MSC proliferation, cells were cultured on TCP and treated with varying concentrations of recombinant human(rh) Cyr61 (0 to 300 μg/mL). After 7 days in culture, proliferation was significantly increased at Cyr61 concentrations of 100 μg/mL and higher, achieving a plateau between 100 and 300 μg/mL, but failed to reach the level observed on yECM alone (Fig. 5A). To determine whether exogenous rhCyr61 was able to promote BMP-2 responsiveness of the BM-MSCs, cells were cultured on yECM alone or on TCP or eECM in the absence or presence of 100 μg/mL rhCyr61. After 7 days in culture, the growth media were replaced with low serum-containing media (2% FBS) for 24 h and then treated with BMP-2 for 48 h. Based on Runx2 expression, BMP-2 responsiveness was not restored by addition of exogenous rhCyr61 to the cultures on TCP and eECM and only BM-MSCs maintained on yECM responded to BMP-2 treatment by upregulating Runx2 expression (Fig. 5B).

To determine if exogenous rhCyr61 is capable of either adhering or being incorporated into the ECM and altering matrix function, eECM was incubated with varying doses of rhCyr61. After 12 h of incubation at 37 °C, the content of Cyr61 protein in the matrix

was assayed by Western blot, using Cyr61 content in yECM as a reference (Fig. 5C). As indicated previously, yECM contained significantly more Cyr61 than eECM. In addition, soluble rhCyr61 protein, incubated directly with the matrices, did not become incorporated into the matrix.

Incorporation of Cyr61 into the ECM can be down- or up-regulated by genetic modification during matrix synthesis

To better understand the sequence of events that result in Cyr61 incorporation into the ECM, dynamic changes in Cyr61 gene expression were measured at three timepoints during ECM synthesis. The first time point (−1 day, pre-ECM induction), reflects the level of gene expression as the cells reach confluence and prior to the addition of ascorbic acid to induce ECM synthesis. The second time point (+1 day, post-ECM induction), reflects the level of gene expression after one full day of producing the ECM. The final time point (+3 days, cessation of ECM synthesis and harvest), reflects the level of gene expression three days after inducing ECM synthesis (Fig. 6A). At all times during the study, Cyr61 expression was always higher in untreated young versus elderly BM stromal cells. To downregulate (i.e. knockdown) the expression of Cyr61 in young BM stromal cells, cultures were treated with Cyr61 siRNA ($siRNA^{Cyr61}$) or scrambled siRNA ($siRNA^{Scr}$) as a negative control. Conversely, to upregulate the expression of Cyr61 in elderly BM stromal cells, cultures were infected with an adenoviral vector carrying the Cyr61 (AdV^{Cyr61}) gene or a null vector (AdV^{Null}) as a negative control. When these approaches were employed, treatment with $siRNA^{Cyr61}$ reduced Cyr61 transcription in young cells to levels even lower than those of the control (untreated) elderly BM stromal cells. In contrast, infection of elderly BM stromal cells with the AdV^{Cyr61} successfully increased Cyr61 expression, immediately preceding and following induction, to levels higher than those of young cells before reaching an equivalent expression level at the time of ECM harvest (Fig. 6A).

To confirm that changes in Cyr61 gene expression resulted in altered incorporation of Cyr61 protein in the matrix, we prepared protein lysates of decellularized young- and elderly ECMs (naïve or after treatment with $siRNA^{Cyr61}$ or AdV^{Cyr61}) for Western blot analysis (Fig. 6B). Young BM stromal cells from three young donors were treated with $siRNA^{Cyr61}$ during matrix production. In each of the cultures, treatment with siRNA significantly reduced the incorporation of Cyr61 into the matrix compared to naïve yECM produced by untreated cells from the same donor. In contrast, elderly BM stromal cells from five donors that had been infected with AdV^{Cyr61} showed a significant increase in the incorporation of Cyr61 into the matrix as compared to naïve eECM made by cells from the same donor.

Finally, the presence of Cyr61 in the modified ECMs was further confirmed by immunofluorescent staining (Fig. 6C). Treatment of young BM stromal cells with $siRNA^{Cyr61}$ during ECM production reduced the staining intensity of Cyr61 as compared to naïve young cells. In contrast, the intensity of Cyr61 staining in ECM produced by elderly BM stromal cells treated with AdV^{Cyr61} was increased compared to naïve elderly cells (Fig. 6C). Taken together, these results show that genetic approaches can be successfully applied to modify the incorporation of Cyr61 during synthesis of both young and elderly ECMs.

Matricellular Cyr61 is essential for retaining BM-MSC proliferation and growth factor responsiveness

To determine the relative importance of Cyr61 content in the matrix to BM-MSC proliferation, cells were seeded at 4000 cells/cm^2 and cultured for 5 or 7 days on TCP, naïve (yECM, eECM) or Cyr61-modified (yECM^{-61}, eECM^{+61}) matrices (Fig. 7A). On days 5 and 7, cell density on yECM was significantly higher than on TCP, while cell density on eECM was significantly lower. Moreover, cell density on yECM^{-61} was significantly lower than yECM on both days. In contrast, eECM^{+61} consistently showed higher cell density relative to eECM. The results clearly suggest that the ablation of Cyr61 in yECM significantly reduced proliferation, while restoration of Cyr61 (i.e. eECM^{+61}) significantly improved the capacity of eECM to support BM-MSC proliferation.

Cyr61 contains binding motifs for a variety of paracrine growth factors, including the TGF-β superfamily (e.g. BMP-2) and IGF-1. To assess the role of ECM-bound Cyr61 in directing the responsiveness of BM-MSCs to BMP-2, cells were cultured on TCP and naïve and Cyr61-modified matrices for 7 days, treated with BMP-2, and expression of Runx2 and BSP measured by RT-PCR. BM-MSCs cultured on yECM and treated with BMP-2 displayed a significant increase in the expression of Runx2 (2.1-fold) (Fig. 7B) and BSP (1.7-fold) (Fig. 7C), while cells cultured on TCP, eECM and yECM^{-61} did not show any significant change in expression. However, BM-MSCs cultured on eECM^{+61} treated with BMP-2 showed a significant upregulation of Runx2 (1.8-fold) and BSP (2.1-fold) expression.

The ability of the different matrices to promote BM-MSC responsiveness to IGF-1 was also assessed based on activation of the Akt pathway (Fig. 8). BM-MSCs cultured on yECM and treated with IGF-1 showed a significantly higher pAkt/Akt ratio than cells on eECM or TCP (Fig. 8A). In the next set of experiments, young BM-MSCs were cultured on naïve (yECM, eECM) and Cyr61-modified matrices (yECM^{-61} and eECM^{+61}), followed by treatment with IGF-1 and preparation of cell lysates and Western blotting (Fig. 8B). In these experiments, cells cultured on yECM^{-61} displayed a significant reduction in sensitivity to IGF stimulation, as compared to cells cultured on yECM. In contrast, cells cultured on eECM^{+61} showed a significant increase in Akt activation (pAkt/Akt) in response to IGF-1, as compared to the cells cultured on eECM.

Both vertebral Cyr61 content and bone mineral density (BMD) decrease with aging in mice

To identify changes in Cyr61 content in skeletal tissue during aging, we first confirmed the normal changes that occur in trabecular bone structure and density in the L4-L5 vertebrae of young (N = 18 C57BL/6 J, 9 males and 9 females, 3–11 m/o) and elderly (N = 7 C57BL/6 J, 2 males and 5 females, 21–33 m/o) mice with μCT. Indeed, the results showed that trabecular bone (L4–5) architecture of young mice was more extensive than that of elderly mice (Fig. 9A). Further, average BMD of the young mice was significantly higher than that of the elderly mice (Fig. 9B). To assess changes in Cyr61 content in these tissues, we harvested and decellularized L4-L5 vertebrae from three young (<4 mo) and four elderly (>21 mo) mice (Fig. 9C, Top). Western blot analysis showed that the abundance of Cyr61 in vertebral bone declined with aging. To ensure that bone samples were completely decellularized and that the observed Cyr61 content was not contributed by

resident cells, GAPDH staining was performed. The results showed no detectable GAPDH in the decellularized bone extracts (Fig. 9C, Bottom). Histomorphometry of the mouse vertebrae revealed a substantial reduction in trabecular structure and thickness in old bone relative to young (Fig. 9D, Top). Importantly, Cyr61 immunohistochemical staining (red) was intense throughout the BM stroma of young vertebrae and bone lining cells (Fig. 9D, Bottom). In contrast, staining in the old vertebrae was notably reduced and nearly absent along the bone interface. These results suggest that the reduction in Cyr61 content in bone matrix with aging may play a role in the loss of vertebral BMD.

Discussion

Previously, we showed that the ECM plays a tissue-specific role in controlling the behavior of BM-MSCs. In addition, our data also indicated that culture on ECM, produced by BM-stromal cells from young donors, improved the quantity and quality of aging BM-MSCs [12,14]. In the present study, we investigated the cues contained within the ECM that are critical for retention of the properties of the BM-MSC niche by preparing ECMs produced by BM stromal cells harvested from “young” versus “elderly” donors. When we compared the phenotype of these young and elderly cells, we failed to detect any differences in MSC surface marker expression (CD73, CD90, and CD105). However, we have previously shown that elderly MSCs are generally less proliferative, display reduced differentiation potential, and produce substantially higher amounts of intracellular reactive oxygen species (ROS) and β-galactosidase, lower levels of ATP, and express decreased amounts of SSEA-4 [14].

In the current study, we compared young BM-MSCs cultured on yECM and eECM and observed that both proliferation and response to BMP-2 and IGF-1 were significantly reduced with culture on the elderly matrices. (Fig. 1A–C). These changes to the BM niche support prior observations that there is an age-related reduction in BM-MSC responsiveness to BMP-2 [52,53] and explain why supraphysiological concentrations of BMP-2 are required to repair bone defects in the elderly [54,55].

To test if differences between y- and e-ECMs altered the fate of BM-MSC differentiation, we treated cells with rosiglitazone (Rgz) and observed that adipogenesis was increased in BM-MSCs maintained on eECM (Fig. 1D). These results correspond to previous, *in vivo* observations, demonstrating an aging-associated decline in BM-MSC number, reduced osteogenesis, and increased adipogenesis [4–7]. Moreover, these findings suggest that ECMs produced by young and elderly BM stromal cells may faithfully reproduce certain physiological attributes of the young and aging BM niche, respectively [56–58].

To identify specific components of yECM versus eECM that might account for their different properties, we comprehensively compared their protein compositions by proteomic analysis (Fig. 3). Although over 70% of the individual protein components were shared by both yECM and eECM, their relative proportions varied over a 4- to 5-fold range (Fig. 3A,B). For example, collagens I and VI were present in both ECMs, but the former predominated in yECM, while the latter was more abundant in eECM. Collagen I is a major component of the BM niche and has been shown to promote osteogenic differentiation of BM-MSCs and support matrix mineralization via $\alpha_v\beta_3$ integrin-mediated activation of

the ERK pathway [59–61], while collagen VI has been found to play a key role in a variety of cytoprotective functions, including inhibition of apoptosis, mitigation of oxidative stress, and regulation of cellular autophagy [62] We found that eECM was enriched in proteoglycans relative to yECM (Fig. 3B), including perlecan (HSPG2), fibulin-2 (FBLN2) and lumican (LUM) (Fig. 3B–C), which are involved in organizing and reinforcing the microfilament assembly of collagen VI. Depletion of collagen I, in concert with an upregulation in collagen VI and associated proteoglycans and glycoproteins, provides additional evidence that remodeling of the collagenous matrix is one of the major events that occurs in the BM niche with aging [63,64] These alterations in the BM-MSC matrisome likely contribute to the distinct differences in architecture and mechanical properties displayed by young and elderly ECMs (Fig. 2).

However, the two most abundant proteins identified exclusively in yECM were CCN-family members Cyr61 (CCN1) and CTGF (CCN2) (Fig. 3D). While both have been shown to play an important role in skeletal development, we limited the scope of this study to CCN1 due to its abundance in yECM, its association with osteogenic differentiation in BM-MSCs, and the gap in knowledge regarding the regulatory role of intracellular versus ECM-bound Cyr61 [43,44,65].

In contrast to ECM structural proteins (e.g., collagens), Cyr61 is a matricellular protein that primarily plays a local regulatory role, directing cell function by binding membrane receptors and/or serving as a cofactor in signal transduction [15,16,18]. In osteoblast-like cells, Cyr61 binds integrin $\alpha_v\beta_3$ to promote cell proliferation, differentiation, and BMP-2 expression [66], while binding to integrin $\alpha_6\beta_1$ triggers apoptotic and senescence pathways [25]. Cyr61 contributes to bone anabolism and is a direct target of the Wnt pathway and Wnt-mediated osteoblast differentiation, which is inhibited by Cyr61-knockdown [43]. While a precise mechanism for the role of ECM-bound Cyr61 in osteogenesis remains to be fully elucidated, converging sources point to its critical role in maintaining skeletal homeostasis. Mice with a gain-of-function mutation in the Wnt co-receptor, LRP5, exhibit a high bone mass phenotype and show significant upregulation of Cyr61 gene expression [67]. Exogenous Cyr61 has also been shown to promote fracture healing in rabbits, while siRNA inhibits bone regeneration in a murine model [48,68]. Moreover, the absence of Cyr61 is associated with defects in bone development and skeletal homeostasis [51]. While these studies demonstrate the importance of intracellular Cyr61 in regulating bone maintenance, none has specifically addressed the role of ECM-bound Cyr61 in regulating osteogenesis. In the present study, we hypothesized that ECM-bound Cyr61 is an important component of the BM niche (or microenvironment) that plays an essential role in maintaining the resident stem cells and their properties.

Our results show that young BM-MSCs produce higher levels of Cyr61 than elderly BM-MSCs (Fig. 4A) and that these differences were reflected in the abundance of Cyr61 incorporated into the young and elderly ECMs (Fig. 4B and C). To determine if exogenous Cyr61 was capable of reversing the age-related dysfunction of eECM, we added varying amounts of rhCyr61 to cultures of BM-MSCs on TCP or eECM and assessed proliferation and growth factor responsiveness (Fig. 5A). Although addition of rhCyr61 modestly increased proliferation, none of the doses tested stimulated the cultures to attain a cell

density equivalent to that observed on yECM. Similarly, for the BMP-2 responsiveness assays, the addition of exogenous rhCyr61 to cultures of cells on TCP and eECM was less effective than observed on yECM (Fig. 5B). Subsequently, we showed that the addition of exogenous protein to Cyr61-deficient eECMs failed to incorporate into the matrix (Fig. 5C), indicating that for Cyr61 to be a functional component of the BM-MSC niche, it must be incorporated into the matrix by the cells during ECM synthesis.

To precisely demonstrate a role for Cyr61 in the BM-MSC niche, we successfully modified the amount of Cyr61 incorporated into the ECM by down-regulation of young cells with siRNA or up-regulation of elderly cells with an adenoviral vector carrying the Cyr61 gene, respectively (Fig. 6). Functionality of the modified ECMs was initially assessed by measuring BM-MSC proliferation after 5 and 7 days in culture (Fig. 7A). After both times in culture, BM-MSC proliferation on yECM^{-61} was significantly lower than on yECM and equivalent to that found on eECM at day 5. Conversely, proliferation on eECM^{+61} was consistently higher than on eECM. These results suggested that the decrease in BM-MSC proliferation seen with maintenance on eECM could be partially restored by culture on ECM produced by elderly BM stromal cells infected with the Cyr61 gene prior to ECM synthesis. However, full recovery of eECM functionality, with the ability to support cell proliferation equivalent to that of yECM, likely requires restoration of additional cues (i.e. protein composition and architectural and mechanical properties) that remain to be identified.

Since Cyr61 contains binding domains for both BMP and IGF, it is possible that Cyr61 in the BM-MSC niche is responsible for binding these growth factors and mediating interactions with their respective receptors [20,69]. With this in mind, we tested whether BM-MSCs cultured on genetically modified ECMs, with up- or down-regulated Cyr61 incorporation, were capable of altering responsiveness to these two growth factors. Indeed, we observed a statistically significant up-regulation of the master osteogenic transcription factor, Runx2, and a mature osteoblast marker, BSP, only on yECM and eECM^{+61} (Fig. 7B and C). Moreover, cells cultured on yECM^{-61} and eECM were equally unresponsive to BMP-2, indicating that ECM-bound Cyr61 directs BM-MSC responsiveness to these osteogenic growth factors. It has been suggested that Cyr61 may bind BMPs via its vWC domain [69]. In the stem cell niche, this interaction may transiently concentrate BMPs around cells or directly facilitate binding to BMP receptors.

Similarly, the response of BM-MSCs to IGF-1 was greater on yECM than on TCP or eECM (Fig. 8A). While cells on yECM^{-61} displayed impaired Akt activation (i.e. pAkt) relative to those on yECM, restoration of Cyr61 to eECM (i.e. eECM^{+61}) appeared to substantially improve the capacity of the cells to respond to IGF-1 (Fig. 8B). As with BMP-2 responsiveness, the data suggest that matrix-bound Cyr61 may play an important role in the ECM by coordinating growth factor activity and/or presentation to the receptor. While the IGFBP domain of Cyr61 has not been conclusively determined to bind IGF-1, it is possible that it mediates receptor-binding through interactions with IGF-1 [70,71]. Taken together, the results suggest that ECM-specific alterations in the aging stem cell niche likely attenuate the sensitivity of BM-MSCs to these critical growth factors.

To determine whether decreased amounts of Cyr61 are found in aging ECM *in vivo*, we compared L4-L5 vertebral bodies from “young” (9–11 m/o) and “elderly” (21–33 m/o) mice and found that tissues with lower BMDs also exhibited a relative deficiency of Cyr61 in the vertebral bone matrix (Fig. 9C and D). Vertebral bodies were selected for the assessment of bone mineral density, architecture and Cyr61 content because they are mainly comprised of dense cancellous bone that changes considerably during growth [72].

Based on these observations, we propose a model which explains how matricellular Cyr61 retains the properties of the BM-MSC niche in bone (Fig. 10). When Cyr61 is produced by cells, a fraction of the total protein exists within the cytosol, where it is involved in signaling (e.g. Wnt pathway) [43]. However, another fraction is also secreted into the extracellular microenvironment [19]. This secreted form of Cyr61, which we have defined as matrix-bound Cyr61, participates in a number of different roles in the ECM. First, it assists in organizing the fibrillar architecture of the matrix and maintaining its mechanical properties. To accomplish this, binding motifs in the TSR and CT domains interact with structural proteins in the matrix, such as fibronectin, vitronectin, collagens, small leucine-rich proteoglycans (e.g. decorin and biglycan), and heparan sulfate proteoglycans (e.g. perlecan and syndecan) [16–19]. Second, although Cyr61 lacks an RGD-binding sequence, its vWR, TSR and CT domains contain diverse binding motifs, which engage with a variety of integrins (i.e. $\alpha_v\beta_3$, $\alpha_v\beta_3$) and receptors (e.g. LRP1), and participate in cellular mechanotransduction and the regulation of diverse cellular functions [20]. Third, Cyr61 may act as a “signal amplifier” and assist in targeting growth factors to cells. The vWC subunit contains binding elements for the TGFβ superfamily, while the IGFBP subunit interacts with IGFs [20]. In our studies, cells cultured on Cyr61-containing ECMs display increased responsiveness to both BMP-2 and IGF-1 which may be due to Cyr61 acting as a co-receptor and/or autocrine or paracrine reservoir. Aging processes decrease the expression of Cyr61 which may be associated with changes in the expression of Yes-associated protein (YAP), one of the chief transcriptional regulators of cellular mechanotransduction and a key co-activator of the Hippo growth-regulatory pathway [72]. In its phosphorylated form, p-YAP is sequestered in the cytoplasm and transcriptionally inactive. However, when de-phosphorylated, “active” YAP is translocated into the nucleus, where it interacts with a number of transcription factors to activate the expression of growth-related genes, including Cyr61. Recently, nuclear translocation of YAP has been shown to progressively decline with age [47,73], suggesting a possible mechanism responsible for the reduced incorporation of Cyr61 into eECM by elderly BM-MSCs. In addition, the expression of Runx2 and Osterix, which may regulate Cyr61 super enhancers, has been shown to decline with age in C57BL/6 mice [74].

Both *in vitro* [77,78] and *in vivo* [79,80] models have demonstrated that combined treatment with BMP-2 and IGF-1 synergistically promotes osteoblast differentiation. In fact, recent bone implant studies have suggested that it may be possible to reduce the dose of BMP-2 required to obtain bone healing when co-administered with IGF-1 [81]. In aging bone, the gradual depletion of Cyr61 in the microenvironment may reduce the ability of resident MSCs to respond to BMP-2 and IGF-1, promoting bone degeneration, reduced osteogenesis, and osteopenia [75,76]. Our results suggest a new paradigm for addressing the deleterious effects of aging on the bone microenvironment by treating age-related bone loss through

the restoration of key ECM components, such as Cyr61, using drug delivery vehicles (e.g. scaffolds or nanoparticles) and/or gene therapies. This approach, when properly targeted, has the potential to restore the stem cell niche and promote *in situ* tissue regeneration by mobilizing the endogenous stem/progenitor cells to restore tissue homeostasis which has been perturbed by aging or degenerative disease.

Materials and methods

Preparation of BM-MSCs

Human BM aspirate from healthy young donors (≤25 years old) was purchased from Lonza Group Ltd. (Walkersville, MD, USA; see: https://www.lonza.com for IRB information) and young BM-MSCs harvested in our lab as described previously [82,83]. Briefly, fresh BM extracts, containing primary BM-MSCs, were seeded into standard, tissue culture plastic (TCP) vessels (Millipore-Sigma, St. Louis, MO) at 5×10^5 cells/cm^2. Cells were cultured in "growth media" consisting of α-MEM (Life Technologies, Grand Island, NY) containing glutamine (2 mM), penicillin/streptomycin, and 15% fetal bovine serum (FBS) (Atlanta Biologicals, Lawrenceville, GA). Half-volume changes of growth media were performed every 3–4 days until 70–80% confluence was achieved (2–3 weeks). During culture, non-adherent cells were removed by phosphate buffered saline (PBS) washing and adherent cells (passage 1; P1 cells) collected by trypsinization. The BM-MSC phenotype was confirmed by expression (>90%) of CD73, CD90, and CD105 and negative selection for CD34, CD45 and HLA-DR.[84]. Cells were either used immediately in the experiments or frozen in liquid nitrogen (LN_2) for later use.

Elderly BM was procured, as described previously [14], from male and female patients (≤60 years old) undergoing total knee or hip arthroplasty, after providing informed consent (Protocol approval was obtained from the UTHSCSA IRB) and processed. Samples of cancellous bone from the surgical site (typically discarded) were collected in isolation buffer (Hank's Buffered Saline Solution +5% (v/v) fetal bovine serum) and maintained at 4 °C. Within 3–4 h, the bone samples were trimmed and diced into small pieces, and then digested with collagenase (type 2; 400 units/ml) for 30 min at 37 °C. This digest was centrifuged (600 × g) for 5 min at 4 °C. The resulting pellet was re-suspended in isolation buffer and then washed three times with cold PBS before filtering to remove any remaining bone fragments with a 100 μm pore-size cell strainer. Next, this filtrate was centrifuged (600 × g, 5 min) to collect BM mononuclear cells and the pellet resuspended in growth media. The resulting cells were seeded (5×10^5 cells/cm^2) into TCP flasks and cultured in growth media (see above) until colonies formed. Once colonies appeared, full media were removed, nonadherent cells washed away, and fresh media added. These cells were expanded (P1/P2), immunophenotyped for MSC marker expression as above, and used immediately or frozen in LN_2.

Preparation of cell-free BM yECM and eECM

Young and elderly ECMs (yECM, eECM) were prepared using BM stromal cells, as described previously [8,82,83], and stored dry. Briefly, BM stromal cells, isolated as described above, were seeded in 6-well tissue culture plates at 6×10^3 cells/cm^2 and

cultured in “growth media” for 15 days, with media changes every 3–4 days. On day 8 of culture, ascorbic acid (50 μM) (Millipore-Sigma) was added to the media. On day 15, the ECMs were washed with PBS, followed by decellularization with 0.5% Triton X-100 and 20 mM NH_4OH in PBS, by incubation for 5 min at 37 °C. The decellularized ECM was rinsed 3 times with PBS, followed by sterile distilled water and then allowed to dry at room temperature before storing at 4 °C. Immediately before use, the ECMs were re-hydrated with PBS for 1 h at 37 °C. To ensure the reproducibility of ECMs produced by cells from a particular donor and minimize both intra- and inter-batch variation, quality control measures described in our previous studies were employed [82,83]. These included the use of standardized seeding densities, consistent culture durations for ECM production, and well-established decellularization protocols. These measures have been used in our laboratory for over 10 years for the production of reproducible, cell-elaborated culture substrates, while preserving the natural variation due to differences in the donors and their physiological states (i.e. aging).

Analysis of cell behavior on ECMs

Young BM-MSCs were used in all experiments evaluating cell behavior on yECM, eECM, or their modified derivatives, $yECM^{-61}$ and $eECM^{+61}$. Cells were sourced from a young donor (≤25 years old) and frozen in aliquots for future use at passage 3 (P3). For use in the experiments, the cells were thawed and expanded from this stock of cells.

Analysis of cell proliferation

Young BM-MSCs were seeded at 2.5×10^3 cells/cm^2 on yECM, eECM or TCP and cultured for 5 days in growth media. At harvest, cells were detached from TCP surfaces with trypsin and detached from ECMs with collagenase. Cells were stained with trypan blue and counted using a hemocytometer.

Assessment of BM-MSC-responsiveness to treatment with osteogenic (rhBMP-2) and adipogenic (Rgz) inducers

Response of young BM-MSCs to treatment with rhBMP-2 (200 ng/mL) and Rgz (1.9 μg/mL) was assessed as previously described using RT-PCR and primers for markers of osteogenesis and adipogenesis [82].

Quantification of gene expression

Cells were rinsed with cold PBS and total RNA isolated using the Trizol reagent (Life Technologies, Carlsbad, CA, USA). cDNA was reverse-transcribed from the extracted RNA (2 μg) using a High Capacity cDNA Archive Kit (Applied Biosystems, Foster City, CA, USA). Transcripts of interest and GAPDH were amplified from the cDNA by real-time PCR using TaqMan Universal PCR Master Mix and Assay-on-Demand or Assay-by-Design primer/probe sets (Applied Biosystems). The following primers were used in this study: Runx2 (Hs00231692_m1), BSP (Hs00173720_m1), PPARγ (Hs00234592_m1), Cyr61 (Hs00155479_m1) and GAPDH (Hs02758991_g1). Amplification and detection were carried out with an ABI 7900HT Fast Real-Time PCR System (Applied Biosystems). Gene

expression was quantified by subtracting the GAPDH threshold cycle (Ct) value from the Ct value of the gene of interest, expressed as $2^{-\Delta Ct}$ as per the manufacturer's protocol.

Surface characterization of ECMs

Surface mapping of yECM and eECM was performed using a Veeco MultiMode atomic force microscope (AFM) (Bruker, Santa Barbara, CA, USA) in tapping mode, on non-hydrated ECMs. Fiber orientation was quantified in ImageJ using the OrientationJ directional analysis plug-in (EPFL, Switzerland) as described [83]. ImageJ outputs a frequency of tangents to fibers in 180 bins. Each image was rotated such that the mode was 90°, and the MATLAB distribution toolbox was used to determine the parameters of a normal distribution that would describe the probability distribution with 95% confidence.

Mean average roughness (Ra) of the surfaces was computed using NanoScope software (Bruker, Santa Barbara, CA, USA). Three replicates of each surface were evaluated, and 15 randomly selected areas were measured in each. Surface roughness data represents the mean ± 95% confidence interval of 15 randomly-selected areas from each substrate.

Mechanical characterization of ECMs

The mechanical properties of rehydrated yECM and eECM were measured using an MCR 302 Rheometer (Anton Paar, Austria) with a 25 mm diameter parallel-plate at 37 °C, as previously described [83]. Data points represent the mean ± 95% confidence interval of $N = 4$ ECMs.

Compositional analysis of ECM using mass spectrometry

Mass spectrometric (MS) analysis of the ECMs was performed as previously described [85,86]. ECM proteins were isolated by physical agitation, followed by sonication in PBS. The ECM pellet was treated with Protein Extraction Reagent Type 4 (Millipore-Sigma), dried and reconstituted in Ready Prep 2-D Rehydration Sample Buffer (Bio-Rad Laboratories, Hercules, CA, USA). Freeze-thaw cycling and sequential centrifugation produced two supernatants, with the intermediate pellet dissolved in 100 μL DMSO. The two supernatants were each adjusted to 8 M urea and then combined. A 200 μL aliquot of the resulting sample was then vortexed with 1 mL acetone and stored overnight at 4 °C. The acetone supernatant was removed by re-centrifugation, and the pellet was air-dried at room temperature. Dried samples were reconstituted in 50 μL 2x SDS buffer and boiled at 100 °C for 5 min before loading onto an SDS-PAGE gel.

Protein separation was performed using onedimensional SDS-PAGE and Coomassie blue staining. Proteins were released from discrete serial sections of each lane of the gel by *in situ* trypsin digestion. Digests were analyzed using capillary HPLC-electrospray ionization tandem mass spectrometry (HPLC-ESI-MS/MS) on a Thermo Fisher LTQ fitted with a New Objective PicoView 550 nanospray interface. On-line HPLC separation of the digests was accomplished with an Eksigent NanoLC micro HPLC. A mass spectral scan strategy was used in which a survey scan was acquired followed by data-dependent collision-induced dissociation (CID) spectra of the seven most intense ions in the survey scan. Mascot (Matrix Science) was used to search the mass spectra against the SwissProt database. Methionine

oxidation was considered as a variable modification. Cross correlation of the Mascot results with X! Tandem and determination of protein and peptide identity probabilities were accomplished by Scaffold (Proteome Software). Protein identifications were accepted using the following criteria: minimum of 2 peptides; peptide probability, ≤ 95%; protein probability, ≤ 99%. Protein components identified in the ECMs were ontologically classified with the Enrichr gene analysis tool (https://maayanlab.cloud/Enrichr/) using the Jensen TISSUES, tissue-specific gene expression database (https://tissues.jensenlab.org/).

Western blot analysis of cell, ECM and bone tissue protein extracts

For cell protein extracts, cells were washed with cold PBS and lysed with RIPA buffer supplemented with protease inhibitor cocktail (cOmplete™, Roche, Switzerland), reconstituted in 1 mM EDTA. Dishes were agitated for 30 min at 4 °C and the cell lysates collected. Cyr61 band densitometry was quantitated relative to GAPDH.

Extraction of ECM proteins was performed using a modification of the method reported by Zhang et al. [23]. Briefly, decellularized ECMs were washed twice with PBS and the matrix harvested by scraping in the presence of 100 μL extraction buffer consisting of 0.5 M Tris–HCl (pH 6.8), 10 M urea, 10% SDS, 1 M DTT, and protease inhibitors. Protein extracts were homogenized on ice with a probe sonicator (D100, Fisher Scientific, Waltham, MA, USA) at 5 Watts output for 15 s. Samples were boiled at 100 °C for 10 min, immediately placed on ice, and then centrifuged at 12000x g for 5 min. The supernatants were stored at −80 °C.

To extract protein from lumbar vertebrae, young and elderly mice were euthanized and the lumbar vertebrae (L4–5) removed, cleaned of soft tissue, and frozen in LN2. Frozen vertebrae were homogenized with a grinder, decellularized with sterile distilled water, and then spun down to remove soluble material (i.e. supernatant). Pellets were re-suspended in lysis buffer (5 mM Tris, EDTA/EGTA, 1% SDS and proteinase inhibitors). The protein fractions were then heated at 100°C for 10 min, placed on ice, followed by centrifugation at 12000x g for 15 min at 4 °C. The supernatants were stored at −80°C until they were assayed for Cyr61 by WB.

Protein extracts (20 μg) were resolved on mini-format bis/polyacrylamide gels (Bio-Rad Laboratories) for 5 min at 50 V, before increasing to 100 V for 1 h. Protein gels were placed in 1x transfer buffer for 15 min and proteins transferred onto 0.2 μm PVDF membranes at 100 V for 1 h (Bio-Rad Laboratories). Membranes were placed in 4% milk blocking solution for 1 h, then probed overnight at 4 °C with the following primary antibodies (Cell Signaling Technology, Rabbit): Cyr61 (mAb #14,479); GAPDH (mAb #97,166); Akt (mAb #9272); Akt Phospho-Akt Ser473 (mAb #9271). Optical density of band staining was quantified using FIJI image analysis software. For both ECM and tissue-derived protein extracts, GAPDH bands were shown to indicate successful decellularization and not used for reporting Cyr61 band density.

Immunofluorescent (IF) staining of ECMs

ECMs were rehydrated and then treated with DNase (100 units/mL; Millipore-Sigma) as described [83]. After removal of the enzyme and a brief rinse in PBS, the ECMs were

fixed with 4% paraformaldehyde/PBS, washed with PBS, and then stored in PBS until staining [83]. For IF staining, ECMs were first treated with blocking solution (Bloxall, Vector Laboratories, Inc., Burlingame, CA) and then incubated for 1 h at 4 °C with primary antibody specific for human Cyr61 (1:450 dilution; polyclonal rabbit IgG; Santa Cruz Biotechnology, Dallas, TX). Non-specific rabbit IgG (Millipore-Sigma) was employed as a negative control (1:200). Unbound primary antibody was removed by washing with cold (4 °C) PBS. After washing, the ECMs were incubated with blocking solution again for 10 min at room temperature. Secondary antibody (1:200; FITC-conjugated goat anti-rabbit IgG, Millipore-Sigma) was then added and the incubation continued for 1 h at 4 °C. Florescence microscopy was performed at 10x magnification using an Olympus IX73 inverted microscope. Quantification of immunofluorescent staining was performed by assessing optical density of 15 randomly-selected areas from three replicates. Optical density of stained pixels was computed by mean gray value in FIJI image analysis software.

Assessment of exogenous rhCyr61 on BM-MSC proliferation

Young BM-MSCs were seeded (2.5×10^3 cells/cm^2) on TCP and yECM and cultured for 5 days. Cells on yECM were cultured in growth media, while cells on TCP were cultured in growth media supplemented with 0 to 300 μg/mL recombinant human Cyr61 (rhCyr61; R&D Systems, Minneapolis, MN, USA). Cells were released from the substrates and counted as described above.

Assessment of the effect of rhCyr61 on BMP-2 responsiveness by BM-MSCs

Young BM-MSCs (P3) were cultured for 7 days as described above. During expansion, three groups of cells on yECM, eECM or TCP were maintained in growth media, while two additional groups cultured on eECM and TCP were supplemented with 100 μg/mL rhCyr61. On day 7, all groups were switched to growth media containing 2% FBS for 24 h. On day 8, 200 ng/mL rhBMP-2 (Life Technologies, Frederick, MD, USA) was added to the media for an additional 48 h. Changes in transcripts in response to BMP-2 treatment were measured using RT-PCR as described above.

Assessment of BM-MSC-responsiveness to IGF-1

Young BM-MSCs (P3) were seeded and cultured as described above. On day 7, the media were switched to growth media containing 2% FBS and the cultures continued overnight. On day 8, 20 ng/μL IGF-1 (R&D Systems, Minneapolis, MN) was added to the cultures for 1 h. Following IGF-1 treatment, cell protein lysates were prepared using RIPA buffer, and probed by WB, as described above. Akt phosphorylation was quantified by comparing the optical density (OD) of pAkt and Akt bands (pAkt/Akt ratio).

Preparation of Cyr61-modified yECM and eECM

For Cyr61-modified ECMs, the procedure described above for producing ECM was adjusted to allow for transfection with siRNA or infection with adenoviral vectors (AdV). For controls, each batch of Cyr61-modified ECMs was paired with the corresponding unmodified yECM or eECM, prepared by cells from the same cell donor.

To produce Cyr61-depleted young ECM ($yECM^{-61}$), the following siRNA reagents were purchased from GE Dharmacon (Lafayette, CO, USA): ON-TARGETplus Human CYR61 SMARTpool (L-004,263–00–0005), siGLO Green Transfection Indicator (D-001,630–01–05), and ON-TARGET-plus Non-targeting Pool (D-001,810–10–05). The transfection reagent was purchased from Invitrogen (Lipofectamine RNAiMAX [Cat#13,778,075]). To produce the modified ECM, young BM stromal cells were cultured for 5 days to 80% confluence, switched to media containing 50 nM of non-targeting or Cyr61-targeting siRNA, incubated at 37 °C for 24 h in the absence of antibiotics/antimycotics, and then reverted to complete growth media for an additional 48 h. On day 8, the cultures were treated with ascorbic acid (50 μM) (Millipore-Sigma) and the cultures continued until the ECM was harvested.

To produce Cyr61-enriched elderly ECM ($eECM^{+61}$), the following adenoviral vectors were purchased from Vector Biolabs (Malvern, PA, USA): human-CYR61 (SKU #ADV-206,536), GFP vector (Cat#1060), and null vector (Cat#1300). Optimization of the AdV concentration for infection was performed as previously described [87]. In brief, BM stromal cells were seeded at 3×10^3 cells/cm^2 and 5×10^3 cells/cm^2, administered the GFP vector at multiplicities of infection (MOI) ranging from 100 to 500, inspected under bright field microscopy for cytotoxicity and FITC for transfection, and sorted based on GFP expression via flow cytometry. The MOI which led to the greatest percentage of GFP-expressing cells without introducing significant toxicity was selected for use in the experiments. To produce the modified ECM, elderly BM stromal cells were cultured for 5 days to 70–80% confluence and then treated with complete growth media containing 1 mL Cyr61 AdV or Null Vector at an MOI of 450 for 24 h followed by a 48 h recovery period as described [62]. On day 8, the cultures were treated with ascorbic acid (50 μM) (Millipore-Sigma) and the cultures continued until the ECM was harvested.

Vertebral BMD measurement by μCT

MicroCT (μCT) analyses were performed on L4 and L5 vertebrae to measure bone mineral density (BMD). All samples were analyzed using a Skyscan 1172 scanner (pixel size resolution of 10.06 μm using 59 kV & 167 uA and an exposure of 800 ms with a rotation step of 0.7°) equipped with a 11 MPix camera. The superior region of interest started 0.20 mm below the growth plate of the L4 vertebral body and ended inferiorly 0.20 mm above the growth plate of the L5 vertebral body. A set of 2 mm diameter hydroxyapatite (CaHA) phantoms was used for calibration and computing volumetric BMD. All images were reconstructed using Skyscan NRecon software.

Vertebral bone tissue histomorphometry and Cyr61 immunohistochemistry

L4-L5 vertebral sections were prepared for histomorphometry and immunohistochemical staining as previously described [66]. Bone samples were fixed in RNase-free 4% paraformaldehyde, demineralized in RNase-free 15% EDTA, and embedded in paraffin. Tissue sections were stained with Hematoxylin & Eosin or prepared for immunohistochemical staining as described previously [83]. Immunostaining of vertebral sections was performed with human Cyr61 antibody (1:450 dilution; polyclonal rabbit IgG; Cat# sc-13,100; Santa Cruz Biotechnology, Dallas, TX, USA); non-specific rabbit IgG (Cat#

12–370; Millipore-Sigma) as a negative control (1:200); and biotinylated goat anti-rabbit IgG (1:200) (Cat# SAB4600006; Millipore-Sigma) as a secondary antibody, followed by incubation with alkaline phosphatase conjugated avidin/biotin complex (Cat# AK-5000; Vector Laboratories). Fast Red substrates were used to develop the alkaline phosphatase staining. Microscopy was performed using an Olympus IX73 inverted microscope and images analyzed using ImageJ software.

Statistical analysis

Two-tailed Student's t-tests were used to determine significance in all pairwise comparisons; $P < 0.05$ considered significant. Error bars in replicate data sets were presented as mean values ± 95% Confidence Interval (CI). All multi-way statistical comparisons were performed using one-way ANOVA with Tukey′s post-hoc test. At a minimum, experimental replicates were performed in triplicate and each experiment was repeated a minimum of 3 times.

Acknowledgements

This study was supported by a VA Merit Review (1I01BX002145-01) to Dr. Chen. Milos Marinkovic was supported by a NIH-NCATS TL1 Translational Science Training grant (TL1 TR001119), NIH-NIDCR F31 National Research Service Award (F31 DE02668) and pilot funding from the San Antonio Nathan Shock Center of Excellence in the Basic Biology of Aging. Mass spectrometry analyses were conducted at the UTHSCSA Institutional Mass Spectrometry Laboratory which is supported in part by an NIH shared instrumentation grant (1 S10 RR021160-01) to Dr. Susan T. Weintraub, Director of the Mass Spectrometry Core Laboratory. The expert technical assistance of Kevin Hakala, M.S. and Sammy Pardo, B.A. in performing the mass spectrometry studies is greatly appreciated. Mouse vertebrae were generously provided by Dr. Adam Salmon at the Barshop Institute for Longevity and Aging Studies at UTHSCSA. The authors express gratitude to Dr. Vaida Glatt at the UTHSCSA Orthopaedic MicroCT core facility for her expertise in BMD imaging and analysis and Jelica Gluhak-Heinrich for expert assistance with vertebral immunostaining.

Data availability statement

All relevant data from this study, including the proteomic data, are available from the corresponding author upon request. The proteomic data will be deposited in a searchable, public database.

References

[1]. Murray IR, West CC, Hardy WR, James AW, Park TS, Nguyen A, et al. , Natural history of mesenchymal stem cells, from vessel walls to culture vessels, Cell. Mol. Life Sci 71 (2014) 1353–1374. [PubMed: 24158496]

[2]. Kfoury Y, Scadden DT, Mesenchymal cell contributions to the stem cell niche, Cell Stem Cell 16 (2015) 239–253. [PubMed: 25748931]

[3]. Sajeesh S, Broekelman T, Mecham RP, Ramamurthi A, Stem cell-derived extracellular vesicles for vascular elastic matrix regenerative repair, Acta Biomater. 113 (2020) 267–278. [PubMed: 32645438]

[4]. Veronesi F, Torricelli P, Borsari V, Tschon M, L Rimondini M Fini, Mesenchymal stem cells in the aging and osteoporotic population, Crit. Rev. Eukaryot. Gene 21 (2011) 363–377.

[5]. Astudillo P, Ríos S, Pastenes L, Pino A, Rodríguez PJ, Increased adipogenesis of osteoporotic human-mesenchymal stem cells (MSCs) characterized by impaired leptin action, J. Cell. Biochem 103 (2008) 1054–1065. [PubMed: 17973271]

[6]. Pignolo RJ, Law SF, Chandra A, Bone aging, cellular senescence, and osteoporosis, J. Bone Miner. Res. Plus 5 (2021) e10488.

[7]. Singh L, Brennan TA, Russell E, Kim JH, Chen Q, Johnson FB, et al. , Aging alters bone-fat reciprocity by shifting in vivo mesenchymal precursor cell fate towards an adipogenic lineage, Bone 85 (2016) 29–36. [PubMed: 26805026]

[8]. Chen XD, Dusevich V, Feng JQ, Manolagas SC, Jilka RL, Extracellular matrix made by bone marrow cells facilitates expansion of marrow-derived mesenchymal progenitor cells and prevents their differentiation into osteoblasts, J. Bone Miner. Res 22 (2007) 1943–1956. [PubMed: 17680726]

[9]. Lai Y, Sun Y, Skinner CM, Son EL, Lu Z, Tuan RS, et al. , Reconstitution of marrow-derived extracellular matrix *ex vivo*: a robust culture system for expanding large-scale highly functional human mesenchymal stem cells, Stem Cells Dev. 19 (2010) 1095–1107. [PubMed: 19737070]

[10]. Antebi B, Zhang Z, Wang Y, Lu Z, Chen XD, Ling J, Stromal-cell-derived extracellular matrix promotes the proliferation and retains the osteogenic differentiation capacity of mesenchymal stem cells on three-dimensional scaffolds, Tissue Eng. 21 (2015) 171–181 Part C.

[11]. Baroncelli M, van der Eerden BCJ, Chatterji S, Trinidad ER, Kan YY, Koedam M, et al. , Human osteoblast-derived extracellular matrix with high homology to bone proteome is osteopromotive, Tissue Eng. 24 (2018) 1377–1389 Part A.

[12]. Sun Y, Li W, Lu Z, Chen R, Ling J, Ran Q, et al. , Rescuing replication and osteogenesis of aged mesenchymal stem cells by exposure to a young extracellular matrix, FASEB J. 25 (2011) 1474–1485. [PubMed: 21248241]

[13]. Hussey GS, Dziki JL, Badylak SF, Extracellular matrix-based materials for regenerative medicine, Nat. Rev. Mater 3(2018) 159–173.

[14]. Block TJ, Marinkovic M, Tran ON, Gonzalez AO, Marshall A, Dean DD, et al. , Restoring the quantity and quality of elderly human mesenchymal stem cells for autologous cell-based therapies, Stem Cell Res. Ther 8 (2017) 239. [PubMed: 29078802]

[15]. Lau LF, Cell surface receptors for CCN proteins, J. Cell Commun. Signal 10 (2016) 121–127. [PubMed: 27098435]

[16]. Leask A, Conjunction junction, what's the function? CCN proteins as targets in fibrosis and cancers, Am. J. Physiol 318 (2020) C1046–C1054 Cell Physiol.

[17]. Leask A, Abraham DJ, All in the CCN family: essential matricellular signaling modulators emerge from the bunker, J. Cell Sci 119 (2006) 4803–4810. [PubMed: 17130294]

[18]. Perbal B, CCN proteins: multifunctional signalling regulators, Lancet 363 (2004) 62–64. [PubMed: 14723997]

[19]. Lau LF, CCN1/CYR61: the very model of a modern matricellular protein, Cell. Mol. Life Sci 68 (2011) 3149–3163. [PubMed: 21805345]

[20]. Holbourn KP, Acharya KR, Perbal B, The CCN family of proteins: structure–function relationships, Trends Biochem. Sci 33 (2008) 461–473. [PubMed: 18789696]

[21]. Chen N, Chen C, Lau LF, Adhesion of human skin fibroblasts to Cyr61 is mediated through integrin α6β1 and cell surface heparan sulfate proteoglycans, J. Biol. Chem 275 (2000) 24953–24961. [PubMed: 10821835]

[22]. Schütze N, Schenk R, Fiedler J, Mattes T, Jakob F, Brenner RE, CYR61/CCN1 and WISP3/CCN6 are chemo-attractive ligands for human multipotent mesenchymal stroma cells, BMC Cell Biol. 8 (2007) 1–8. [PubMed: 17224075]

[23]. Zhang F, Hao F, An D, Zeng L, Wang Y, Xu X, al, The matricellular protein Cyr61 is a key mediator of platelet-derived growth factor-induced cell migration, J. Biol. Chem 290 (2015) 8232–8242. [PubMed: 25623072]

[24]. Kireeva ML, Mo FE, Yang GP, Lau LF, Cyr61, a product of a growth factor-inducible immediate-early gene, promotes cell proliferation, migration, and adhesion, Mol. Cell. Biol 16 (1996) 1326–1334. [PubMed: 8657105]

[25]. Zhang Y, Sheu T, Hoak D, Shen J, Hilton MJ, Zuscik MJ, et al. , CCN1 regulates chondrocyte maturation and cartilage development, J. Bone Miner. Res 31 (2016) 549–559. [PubMed: 26363286]

[26]. Krupska I, Bruford EA, Chaqour B, Eyeing the Cyr61/CTGF/NOV (CCN) group of genes in development and disease: highlights of their structural likenesses and functional dissimilarities, Hum Genom. 9 (2015) 24.

[27]. Latinkic B, Mercurio S, Bennett B, Hirst E, Xu Q, Lau L, et al. , Xenopus Cyr61 regulates gastrulation movements and modulates Wnt signalling, Development 130 (2003) 2429–2441. [PubMed: 12702657]

[28]. Todorovic V, Chen C-C, Hay N, Lau LF, The matrix protein CCN1 (CYR61) induces apoptosis in fibroblasts, J. Cell Biol 171 (2005) 559–568. [PubMed: 16275757]

[29]. Jun JI, Lau LF, The matricellular protein CCN1 induces fibroblast senescence and restricts fibrosis in cutaneous wound healing, Nat. Cell Biol 12 (2010) 676–685. [PubMed: 20526329]

[30]. Emre Y, Imhof B, Matricellular protein CCN1/CYR61: a new player in inflammation and leukocyte trafficking, Semin. Immunopathol 36 (2014) 253–259. [PubMed: 24638890]

[31]. Kular L, Pakradouni J, Kitabgi P, Laurent M, The CCN family: a new class of inflammation modulators? Biochimie 93 (2011) 377–388. [PubMed: 21130134]

[32]. Kurundkar AR, Kurundkar D, Rangarajan S, Locy ML, Zhou Y, Liu RM, et al. , The matricellular protein CCN1 enhances TGF-β1/SMAD3-dependent profibrotic signaling in fibroblasts and contributes to fibrogenic responses to lung injury, FASEB J. 30 (2016) 2135–2150. [PubMed: 26884454]

[33]. Park MH, Kyung Kim A, Manandhar S, Oh SY, Jang GH, Kang L, et al. , CCN1 interlinks integrin and Hippo pathway to autoregulate tip cell activity, Elife 8 (2019) e46012. [PubMed: 31429823]

[34]. Li ZQ, Ding W, Sun SJ, Li J, Pan J, Zhao C, et al. , Cyr61/CCN1 is regulated by Wnt/β-catenin signaling and plays an important role in the progression of hepatocellular carcinoma, PLoS One 7 (2012) e35754. [PubMed: 22540002]

[35]. Zuo GW, Kohls CD, He BC, Chen L, Zhang W, Shi Q, et al. , The CCN proteins: important signaling mediators in stem cell differentiation and tumorigenesis, Histol. Histopathol 25 (2010) 795–806. [PubMed: 20376786]

[36]. Haque I, Mehta S, Majumder M, Dhar K, De A, McGregor D, et al. , Cyr61/CCN1 signaling is critical for epithelial-mesenchymal transition and stemness and promotes pancreatic carcinogenesis, Mol. Cancer 10 (2011) 8. [PubMed: 21232118]

[37]. Park YS, Hwang S, Jin YM, Yu Y, Jung S, Jung S, et al. , CCN1 secreted by tonsil-derived mesenchymal stem cells promotes endothelial cell angiogenesis via integrin αvβ3 and AMPK, J. Cell. Physiol 230 (2015) 140–149. [PubMed: 24909560]

[38]. Dotterweich J, Ebert R, Kraus S, Tower RJ, Jakob F, Schütze N, Mesenchymal stem cell contact promotes CCN1 splicing and transcription in myeloma cells, Cell Commun. Signal 12 (2014) 1–12. [PubMed: 24383791]

[39]. Xu Z, Chen L, Jiang M, Wang Q, Zhang C, Xiang LF, CCN1/Cyr61 stimulates melanogenesis through integrin α6β1, p38 MAPK, and ERK1/2 signaling pathways in human epidermal melanocytes, J. Invest. Dermatol 138 (2018) 1825–1833. [PubMed: 29510193]

[40]. Jun J, Lau L, Taking aim at the extracellular matrix: CCN proteins as emerging therapeutic targets, Nat. Rev. Drug Discov 10 (2011) 945–963. [PubMed: 22129992]

[41]. Borkham-Kamphorst E, Schaffrath C, de Leur EV, Haas U, Tihaa L, Meurer SK, et al. , The anti-fibrotic effects of CCN1/CYR61 in primary portal myofibroblasts are mediated through induction of reactive oxygen species resulting in cellular senescence, apoptosis and attenuated TGF-β signaling, Biochim. Biophys. Acta Mol. Cell. Res 1843 (2014) 902–914.

[42]. Kim KH, Chen CC, Monzon RI, Lau LF, Matricellular protein CCN1 promotes regression of liver fibrosis through induction of cellular senescence in hepatic myofibroblasts, Mol. Cell Biol 33 (2013) 2078–2090. [PubMed: 23508104]

[43]. Si W, Kang Q, Lu HH, Park J, Luo Q, Song WX, et al. , CCN1/Cyr61 is regulated by the canonical Wnt signal and plays an important role in Wnt_3A-induced osteoblast differentiation of mesenchymal stem cells, Mol. Cell. Biol 26 (2006) 2955–2964. [PubMed: 16581771]

[44]. Su JL, Chiou J, Tang CH, Zhao M, Tsai CH, Chen PS, et al. , CYR61 regulates BMP-2-dependent osteoblast differentiation through the αvβ3 integrin/integrin-linked kinase/ERK pathway, J. Biol. Chem 285 (2010) 31325–31336. [PubMed: 20675382]

[45]. Jullien N, Maudinet A, Leloutre B, Ringe J, Häupl T, Marie PJ, Downregulation of ErbB3 by Wnt3a contributes to Wnt-induced osteoblast differentiation in mesenchymal cells, J. Cell. Biochem 113 (2012) 2047–2056. [PubMed: 22274864]

[46]. Yoshida Y, Togi K, Matsumae H, Nakashima Y, Kojima Y, Yamamoto H, CCN1 protects cardiac myocytes from oxidative stress via beta1 integrin-Akt pathway, Biochem. Biophys. Res. Commun 355 (2007) 611–618. [PubMed: 17316559]

[47]. Pelissier FA, Garbe JC, Ananthanarayanan B, Miyano M, Lin C, Jokela T, et al. , Age-related dysfunction in mechanotransduction impairs differentiation of human mammary epithelial progenitors, Cell Rep. 7 (2014) 1926–1939. [PubMed: 24910432]

[48]. Athanasopoulos AN, Schneider D, Keiper T, Alt V, Pendurthi UR, Liegibel UM, et al. , Vascular endothelial growth factor (VEGF)-induced upregulation of CCN1 in osteoblasts mediates proangiogenic activities in endothelial cells and promotes fracture healing, J. Biol. Chem 282 (2007) 26746–26753. [PubMed: 17626014]

[49]. Zhao G, Kim EW, Jiang J, Bhoot C, Charles KR, Baek J, et al. , CCN1/Cyr61 is required in osteoblasts for responsiveness to the anabolic activity of PTH, J. Bone Miner. Res 35 (2020) 2289–2300. [PubMed: 32634285]

[50]. Schutze N, Noth U, Schneidereit J, Hendrich C, Jakob F, Differential expression of CCN-family members in primary human bone marrow-derived mesenchymal stem cells during osteogenic, chondrogenic and adipogenic differentiation, Cell Commun. Signal 3 (2005) 5. [PubMed: 15773998]

[51]. Zhao G, Huang BL, Rigueur D, Wang W, Bhoot C, Charles KR, et al. , CYR61/CCN1 regulates sclerostin levels and bone maintenance, J. Bone Miner. Res 33 (2018) 1076–1089. [PubMed: 29351359]

[52]. Osyczka AM, Damek-Poprawa M, Wojtowicz A, Akintoye SO, Age and skeletal sites affect BMP-2 responsiveness of human bone marrow stromal cells, Connect. Tissue Res 50 (2009) 270–277. [PubMed: 19637063]

[53]. Lee KB, Taghavi CE, Hsu MS, Song KJ, Yoo JH, Keorochana G, et al. , The efficacy of rhBMP-2 versus autograft for posterolateral lumbar spine fusion in elderly patients, Eur. Spine J 19 (2010) 924–930. [PubMed: 20041271]

[54]. Cheng A, Krishnan L, Tran L, Stevens HY, Xia B, Lee N, et al. , The effects of age and dose on gene expression and segmental bone defect repair after BMP-2 delivery, J. Bone Miner. Res. Plus 3 (2019) e10068.

[55]. Yamaji K, Kawanami M, Matsumoto A, Odajima T, Nishitani Y, Iwasaka K, et al. , Effects of dose of recombinant human BMP-2 on bone formation at palatal sites in young and old rats, Dent. Mater. J 26 (2007) 481–486. [PubMed: 17886450]

[56]. Yu B, Wang CY, Osteoporosis: the result of an ‘aged’ bone microenvironment, Trends Mol. Med 22 (2016) 641–644. [PubMed: 27354328]

[57]. Farr JN, Fraser DG, Wang H, Jaehn K, Ogrodnik MB, Weivoda MM, et al. , Senescent osteocytes: do they cause damage and can they be targeted to preserve the skeleton? J. Bone Miner. Res 31 (2016) 1917–1919. [PubMed: 27653182]

[58]. Moerman EJ, Teng K, Lipschitz DA, Lecka-Czernik B, Aging activates adipogenic and suppresses osteogenic programs in mesenchymal marrow stroma/stem cells: the role of PPAR-γ2 transcription factor and TGF-β/BMP signaling pathways, Aging Cell 3 (2004) 379–389. [PubMed: 15569355]

[59]. Hesse E, Hefferan TE, Tarara JE, Haasper C, Meller R, Krettek C, et al. , Collagen type I hydrogel allows migration, proliferation, and osteogenic differentiation of rat bone marrow stromal cells, J. Biomed. Mater. Res 94A (2010) 442–449.

[60]. de M. Pereira D, Eischen-Loges M, Birgani ZT, Habibovic P, Proliferation and osteogenic differentiation of hMSCs on biomineralized collagen, Front. Bioeng. Biotechol 8 (2020) 554565.

[61]. Salasznyk RM, Klees RF, Hughlock MK, Plopper GE, ERK signaling pathways regulate the osteogenic differentiation of human mesenchymal stem cells on collagen I and vitronectin, Cell Commun. Adhes 11 (2009) 137–153.

[62]. Cescon M, Gattazzo F, Chen P, Bonaldo P, Collagen VI at a glance, J. Cell Sci 128 (2015) 3525–3531. [PubMed: 26377767]

[63]. Kram V, Shainer R, Jani P, Meester JAN, Loeys B, Young MF, Biglycan in the skeleton, J. Histochem. Cytochem 68 (2020) 747–762. [PubMed: 32623936]

[64]. Kirby DJ, Young MF, Chapter 16: isolation, production, and analysis of small leucine-rich proteoglycans in bone, Methods Cell Biol. 143 (2018) 281–296. [PubMed: 29310783]

[65]. Chen Y, Du X, Functional properties and intracellular signaling of CCN1/Cyr61, J. Cell Biochem. 100 (2007) 1337–1345. [PubMed: 17171641]

[66]. Yang W, Guo D, Harris MA, Cui Y, Gluhak-Heinrich J, Wu J, et al. , BMP-2 in osteoblasts of periosteum and trabecular bone links bone formation to vascularization and mesenchymal stem cells, J. Cell Sci 126 (18) (2013) 4085–4098 Pt. [PubMed: 23843612]

[67]. Ayturk UM, Jacobsen CM, Christodoulou DC, Gorham J, Seidman JG, Seidman CE, et al. , An RNA-seq protocol to identify mRNA expression changes in mouse diaphyseal bone: applications in mice with bone property altering Lrp5 mutations, J. Bone Miner. Res 28 (2013) 2081–2093. [PubMed: 23553928]

[68]. Frey SP, Doht S, Eden L, Dannigkeit S, Schuetze N, Meffert RH, et al. , Cysteine-rich matricellular protein improves callus regenerate in a rabbit trauma model, Int. Orthop. 36 (2012) 2387–2393. [PubMed: 23001194]

[69]. Chen CC, Lau LF, Functions and mechanisms of action of CCN matricellular proteins, Int. J. Biochem. Cell Biol 41 (2009) 771–783. [PubMed: 18775791]

[70]. Allard JB, Duan C, IGF-binding proteins: why do they exist and why are there so many? Front. Endocrinol 9 (2018) 117.

[71]. Sarkissyan S, Sarkissyan M, Wu Y, Cardenas J, Koeffler HP, Vadgama JV, IGF-1 regulates Cyr61 induced breast cancer cell proliferation and invasion, PLoS One 9 (2014) e103534. [PubMed: 25062088]

[72]. Wu S, Liu Y, Zheng Y, Dong J, Pan D, The TEAD/TEF family protein scalloped mediates transcriptional output of the Hippo growth-regulatory pathway, Dev. Cell 14 (2008) 388–398. [PubMed: 18258486]

[73]. Zhang H, Pasolli HA, Fuchs E, Yes-associated protein (YAP) transcriptional coactivator functions in balancing growth and differentiation in skin, Proc. Nat. Acad. Sci 108 (2011)2270–2275 USA. [PubMed: 21262812]

[74]. Rauner M, Sipos W, Pietschmann P, Age-dependent Wnt gene expression in bone and during the course of osteoblast differentiation, Age 30 (2008) 273–282 Omaha. [PubMed: 19424851]

[75]. Föger-Samwald U, Patsch JM, Schamall D, Alaghebandan A, Deutschmann J, Salem S, et al. , Molecular evidence of osteoblast dysfunction in elderly men with osteoporotic hip fractures, Exp. Gerontol 57 (2014) 114–121. [PubMed: 24862290]

[76]. Föger-Samwald U, Vekszler G, Hörz-Schuch E, Salem S, Wipperich M, Ritschl P, et al. , Molecular mechanisms of osteoporotic hip fractures in elderly women, Exp. Gerontol 73 (2016) 49–58. [PubMed: 26608808]

[77]. Raiche AT, Puleo DA, *In vitro* effects of combined and sequential delivery of two bone growth factors, Biomaterials 25 (2004) 677–685. [PubMed: 14607506]

[78]. Chen FM, Chen R, Wang XJ, Sun HH, Wu ZF, *In vitro* cellular responses to scaffolds containing two microencapulated growth factors, Biomaterials 30 (2009) 5215–5224. [PubMed: 19560814]

[79]. Zhang J, Li J, Jia G, Jiang Y, Liu Q, Yang X, et al. , Improving osteogenesis of PLGA/HA porous scaffolds based on dual delivery of BMP-2 and IGF-1 via a polydopamine coating, Rsc Adv. 7 (2017) 56732–56742.

[80]. Bai Y, Moeinzadeh S, Kim S, Park Y, Lui E, Tan H, et al. , Development of PLGA-PEG-COOH and gelatin-based microparticles dual delivery system and E-beam sterilization effects for controlled release of BMP-2 and IGF-1, Part. Part. Syst. Charact 37 (10) (2020) 2000180. [PubMed: 33384477]

[81]. Park Y, Lin S, Bai Y, Moeinzadeh S, Kim S, Huang J, et al. , Dual delivery of BMP-2 and IGF-1 through injectable hydrogel promotes cranial bone defect healing, Tissue Eng. (2022) Ahead of print, doi: 10.1089/ten.TEA.2022.0002.

[82]. Marinkovic M, Tran ON, Block TJ, Rakian R, Gonzalez AO, Dean DD, et al. , Native extracellular matrix, synthesized *ex vivo* by bone marrow or adipose stromal cells, faithfully directs mesenchymal stem cell differentiation, Matrix Biol. Plus (2020) 100044. [PubMed: 33543037]

[83]. Marinkovic M, Block TJ, Rakian R, Li Q, Wang E, Reilly MA, et al. , One size does not fit all: developing a cell-specific niche for *in vitro* study of cell behavior, Matrix Biol. 52 (2016) 426–441 –54. [PubMed: 26780725]

[84]. Dominici M, Blanc LK, Mueller I, Slaper-Cortenbach I, Marini F, Krause D, et al. , Minimal criteria for defining multipotent mesenchymal stromal cells. The international society for cellular therapy position statement, Cytotherapy 8 (2006) 315–317. [PubMed: 16923606]

[85]. Block T, Creech J, da Rocha AM, Marinkovic M, Ponce-Balbuena D, Jiménez-Vázquez EN, et al. , Human perinatal stem cell derived extracellular matrix enables rapid maturation of hiPSC-CM structural and functional phenotypes, Sci. Rep 10 (2020) 19071 UK. [PubMed: 33149250]

[86]. Ragelle H, Naba A, Larson BL, Zhou F, Prijić M, Whittaker CA, et al. , Comprehensive proteomic characterization of stem cell-derived extracellular matrices, Biomaterials 128 (2017) 147–159. [PubMed: 28327460]

[87]. Li Z, Sharma RV, Duan D, Davisson RL, Adenovirus-mediated gene transfer to adult mouse cardiomyocytes is selectively influenced by culture medium, J. Gene. Med 5 (2003) 765–772. [PubMed: 12950067]

[88]. Meuleman W, Engwegen JY, Gast MCW, Beijnen JH, Reinders MJ, Wessels LF, Comparison of normalisation methods for surface-enhanced laser desorption and ionisation (SELDI) time-of-flight (TOF) mass spectrometry data, BMC Bioinf. 9 (2008) 88.

[89]. Alfassi ZB, On the normalization of a mass spectrum for comparison of two spectra, J. Am. Soc. Mass Spect 15 (2004) 385–387.

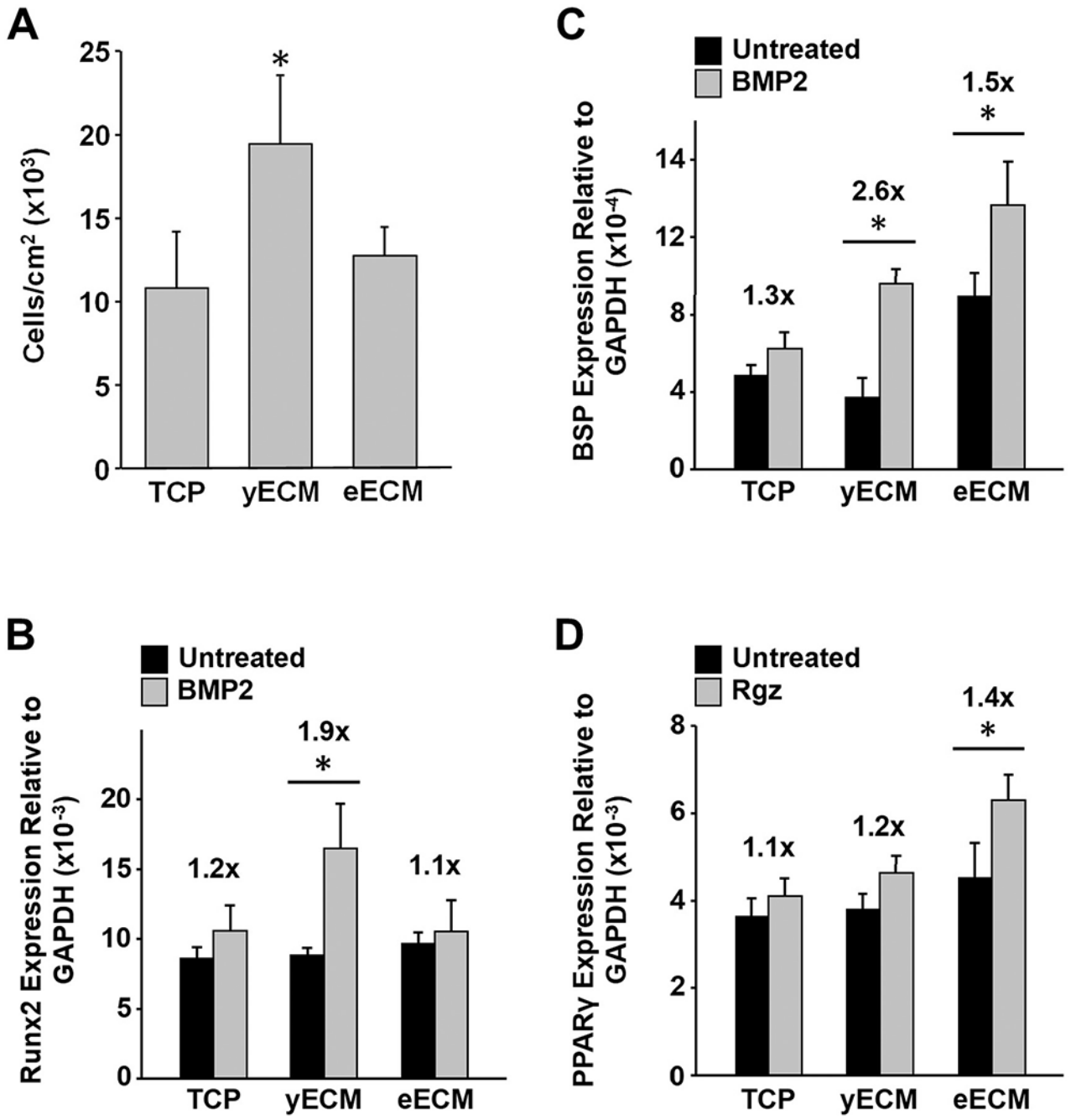

Fig. 1.

Proliferation and response of young BM-MSCs to inducers of osteogenic and adipogenic differentiation during culture on TCP, yECM and eECM. (A) BM-MSCs were cultured on TCP, yECM, and eECM for 5 days, detached from the substrates and then stained with trypan blue for counting. The data are presented as the number of cells/cm2 for each culture surface and reported as the mean ± 95% confidence interval (CI) for $N = 3$ replicates; the experiment was repeated 3 times. $*P < 0.05$, vs. TCP and eECM. (B and C) BM-MSCs were expanded for 7 days on TCP and ECMs produced by cells from three “young” (≤25 y/o)

(=yECM) and three “elderly” (≥60 y/o) (=eECM) donors, switched to low serum-containing media for 24 h, and then treated with BMP-2 (0.2 μg/mL) for 48 h. Changes in Runx2 (B) and BSP (C) expression relative to GAPDH are shown. *$P < 0.05$, vs. untreated control. Fold-change in expression, relative to untreated cells, is indicated above each bar. (D) BM-MSCs were expanded as described in panels B & C, but treated with rosiglitazone (Rgz; 1.9 μg/mL) for the last 48 h. PPARγ expression, relative to GAPDH, is shown. *$P < 0.05$, vs. untreated control. Fold-change in expression, relative to untreated cells, is indicated above each bar.

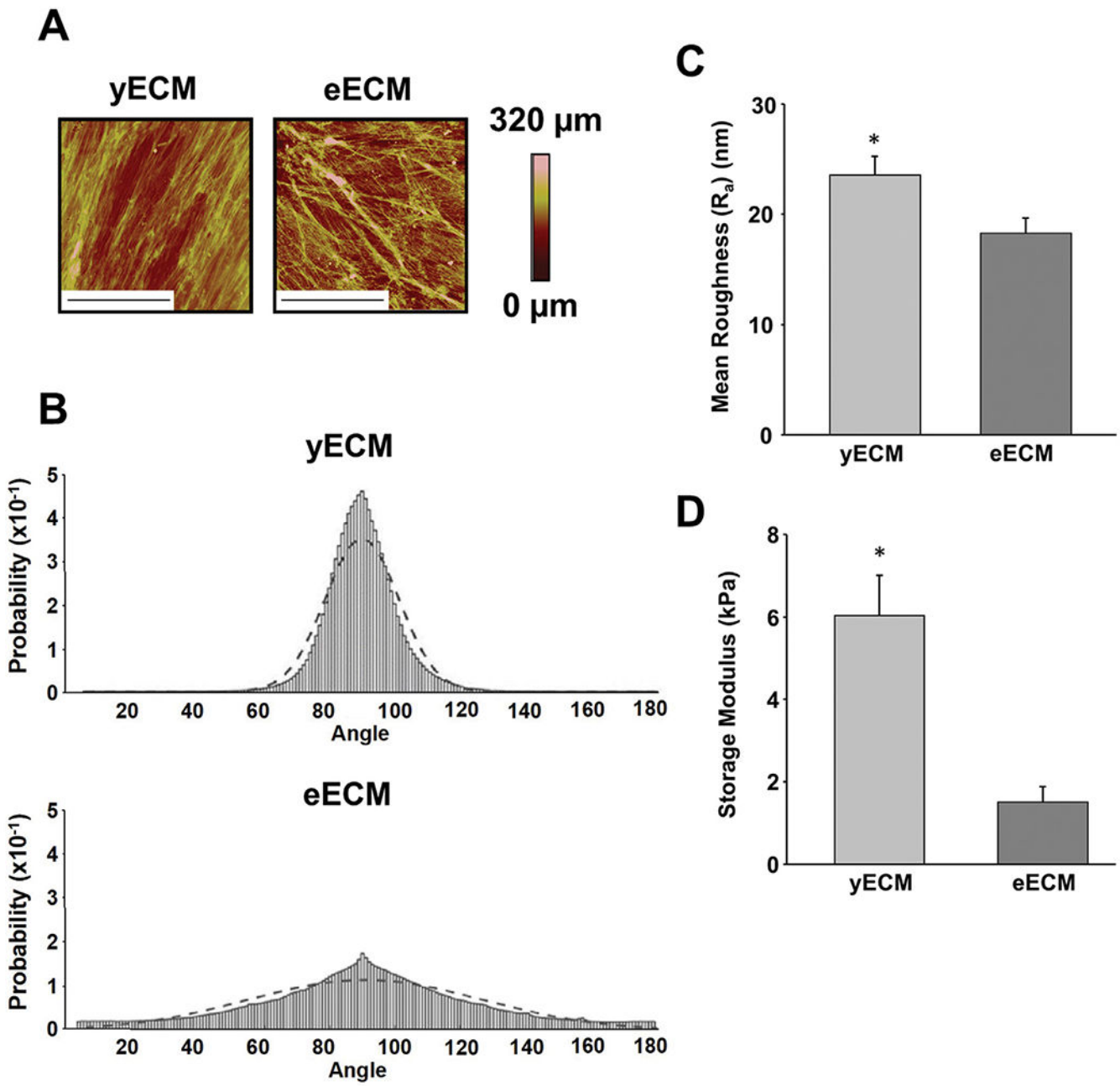

Fig. 2.

Architectural and mechanical characterization of yECM and eECM. (A) High-resolution topographical maps of yECM and eECM were generated using atomic force microscopy (AFM) (tapping mode) and each image represents a 70 × 70 μm region of the matrix. (Bar = 35 μm). The color bar represents changes in height (μm) on the topographical map. (B) Distinct fiber organization was observed in yECM and eECM. Data were fit to a normal distribution, with 90° corresponding to the mode of the observed orientations. A best fit-line for the distribution is overlaid on the raw data. Fibrous structures in yECM displayed a relatively unidirectional (i.e. parallel) alignment (σ = 11.3), while fiber orientation in the

eECM was more variable and widely distributed (σ = 36.3) (i.e. less organized). Mean fiber orientation measurements were performed on 15 randomly selected areas of each ECM (70 μm x 70 μm) using AFM images. (C) Surface roughness (Ra) of yECM and eECM. The arithmetic mean surface roughness for each ECM was computed from AFM (tapping mode) heights generated from 15 randomly selected areas measuring 70 μm x 70 μm. Data represent mean ± 95% confidence interval (CI) for N = 15 replicates from three separate samples of yECM and eECM. *P < 0.05, vs. eECM. (D) Mechanical stiffness of yECM and eECM. The storage modulus was measured by mechanically testing each type of ECM using small angle oscillatory shear rheology (SAOS). Data are reported as the mean ± 95% confidence interval (CI) for N = 4 separate samples of yECM and eECM. *P < 0.05, vs. eECM.

A

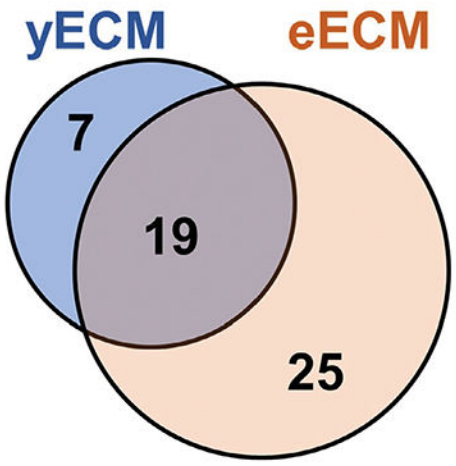

B

ECM Proteins Shared by Young and Elderly Samples (N=4)

Entrez Symbol	yECM	eECM	Fold Change
FN1	6.35E7	8.40E7	-0.40
COL1A1	3.32E7	7.45E6	+2.16
COL1A2	2.77E7	6.41E6	+2.11
COL6A3	2.16E7	1.48E8	-2.78
TNC	1.50E7	1.48E7	+0.01
COL6A2	5.55E6	3.69E7	-2.73
COL6A1	5.30E6	3.17E7	-2.58
COL5A1	4.59E6	2.35E5	+4.29
VCAN	3.64E6	7.01E6	-0.94
HSPG2	2.98E6	6.73E6	-1.17
COL12A1	2.63E6	8.05E7	-4.94
TGFBI	1.05E6	8.68E6	-3.05
COL3A1	7.83E5	9.77E5	-0.32
ANXA2	7.76E5	1.81E7	-4.54
TFPI2	5.60E5	3.75E5	+0.58
ABI3BP	4.93E5	1.75E6	-1.83
EMILIN1	4.38E5	1.47E7	-5.07
BGN	3.31E5	4.82E6	-3.86
DCN	2.60E5	6.61E6	-4.67

C

ECM Proteins Unique to Elderly Samples (N=4)

Entrez Symbol	TIC
FBLN2	1.73E7
POSTN	7.83E6
COL14A1	7.76E6
FBN1	4.56E6
LGALS1	3.21E6
CALR	3.11E6
LUM	2.56E6
MMP2	2.01E6
LAMC1	1.98E6
FBLN1	1.86E6
THBS2	7.92E5
EFEMP2	6.70E5
LAMB1	5.55E5
TIMP1	5.44E5
TNXB	5.19E5
GPC6	4.89E5
SPARC	4.88E5
LGALS3BP	4.43E5
EMILIN2	4.20E5
COL16A1	3.93E5
FMOD	3.78E5
CRTAP	3.39E5
CTHRC1	3.12E5
SERPINF1	2.00E5
PXDN	1.27E5

D

ECM Proteins Unique to Young Samples (N=4)

Entrez Symbol	TIC
CYR61	3.23E6
CTGF	6.23E5
ACAN	5.70E5
MGP	2.76E5
CCDC80	2.13E5
GPC1	2.03E5
COL11A1	1.54E5

Fig. 3.

Proteomic analysis of the yECM and eECM matrisome. (A) Comparison of the protein composition of yECM and eECM using a Venn diagram. Data were obtained from four young and four elderly ECM samples that were each produced by BM-MSCs from individual donors. The ontology of the protein components identified was categorized as corresponding to the ECM using the Enrichr gene analysis tool (https://maayanlab.cloud/Enrichr/) and the Jensen TISSUES, tissue-specific gene expression database (https://tissues.jensenlab.org/). (B) Catalogue of ECM proteins present in both yECM and eECM.

Quantitative data for each protein is represented as total ion current (TIC), in order to normalize the amplitude of MS spectra between samples [88] and transform spectra into a common intensity range suitable for comparison [89]. A fold-change for each protein component was calculated as log2(TIC yECM/TIC eECM). (C) ECM proteins uniquely present in eECM (TIC). (D) ECM proteins uniquely present in yECM (TIC). Cyr61 (CCN1) was the most abundant protein component uniquely present in yECM.

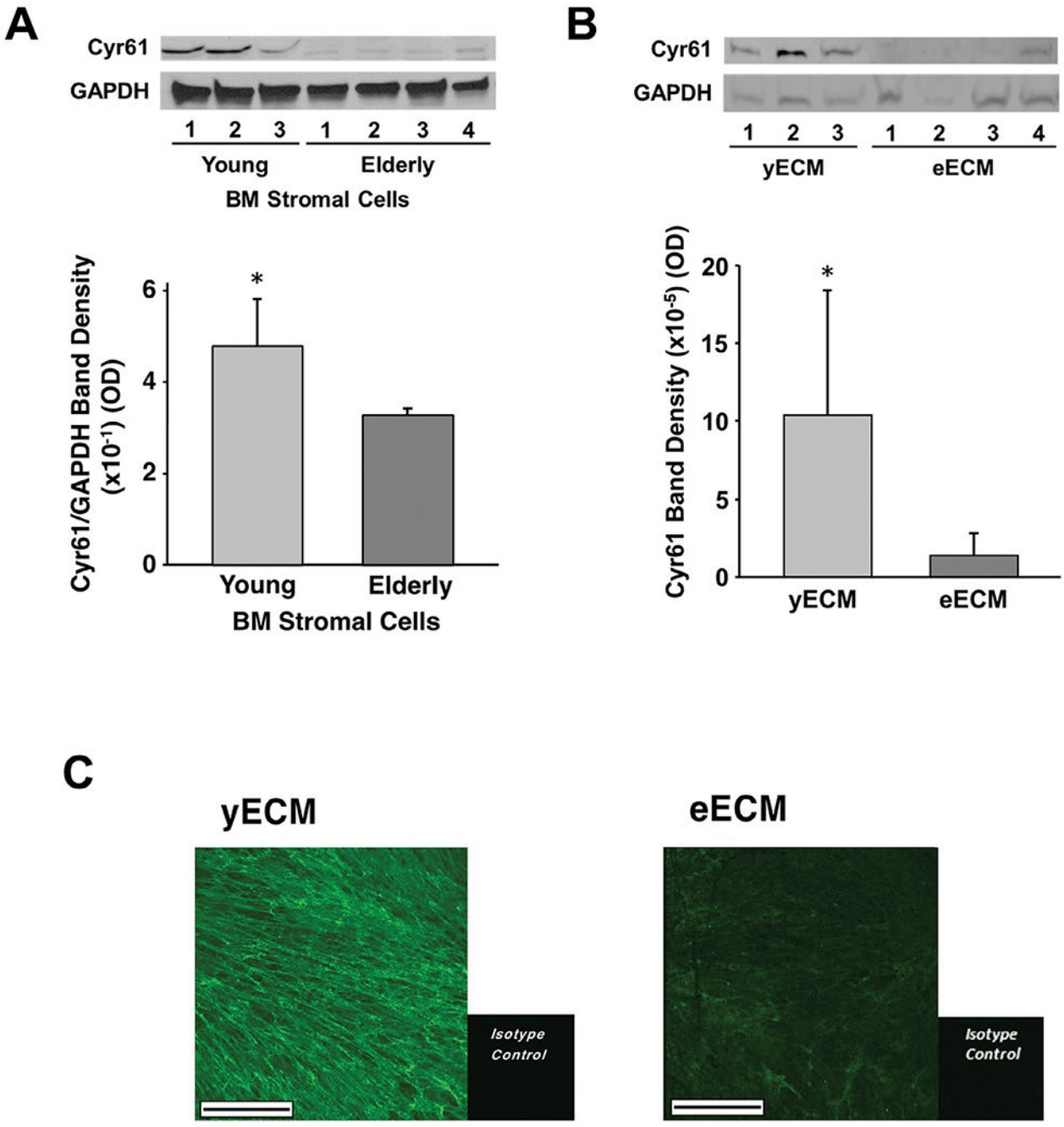

Fig. 4.

Production of Cyr61 protein is substantially reduced in eECM relative to yECM. (A) (Top panel) Protein lysates of BM stromal cells from 3 young- and 4 elderly donors were subjected to gel electrophoresis and Western blot analysis for the presence of Cyr61 using antibodies to Cyr61 and GAPDH (1:450 dilution; polyclonal rabbit IgG). (Bottom panel) Mean band intensity (optical density [OD]) for each lane of the Western blot was quantified using ImageJ software (NIH) and expressed as a ratio of the OD for Cyr61/GAPDH bands. Error bars represent the 95% CI. *$P < 0.05$, vs. Elderly. (B) (Top panel) Protein lysates

of ECMs produced by BM stromal cells from 3 young- and 4 old donors were subjected to gel electrophoresis and Western blot analysis as described in (A) for the presence of Cyr61. (Bottom panel) Mean band intensity for each lane of the Western blot was quantified using Image J as in (A). Error bars represent the 95% CI. *$P < 0.05$, vs. eECM. (C) Immunofluorescence staining for Cyr61 in young and elderly ECMs. Sections were prepared of each ECM, stained using Cyr61 antibody, and then observed using immunofluorescence microscopy. Scale = 100 μm.

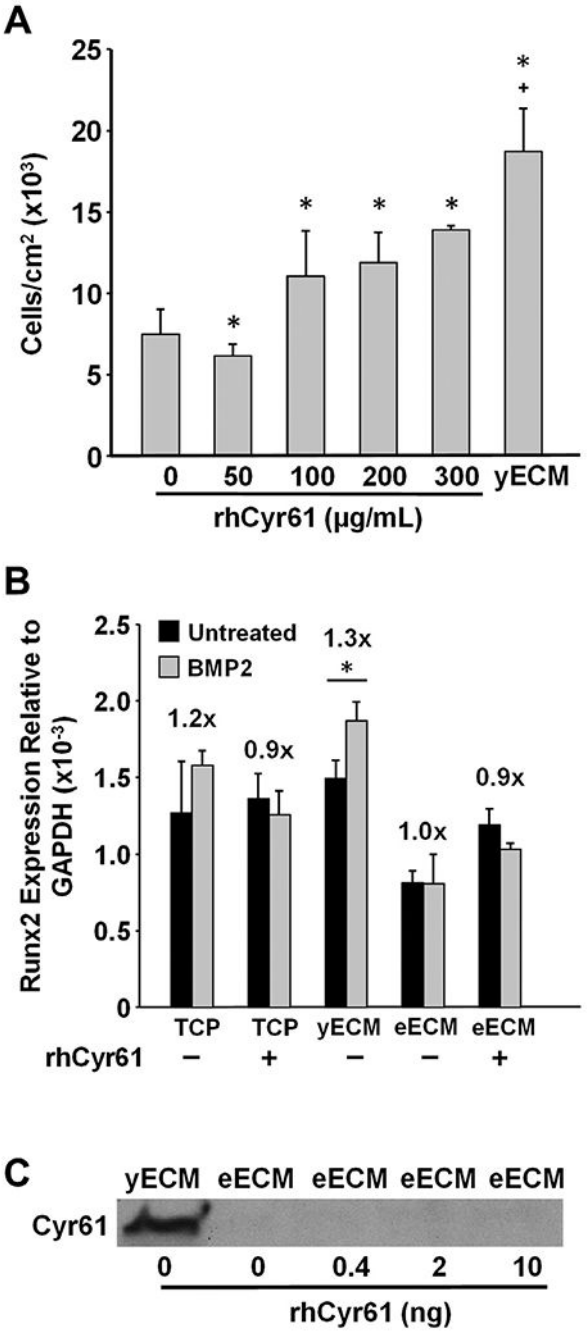

Fig. 5.

Compared to yECM, exogenous rhCyr61 does not stimulate BM-MSC proliferation or promote BMP-2 responsiveness. (A) Effect of exogenous rhCyr61 on BM-MSC proliferation. BM-MSCs were cultured for 7 days on yECM or TCP supplemented with varying amounts of rhCyr61 (50–300 μg/mL). The data are presented as the number of cells/cm^2 and reported as the mean ± 95% confidence interval (CI) for $N = 3$ replicates. *$P < 0.05$, vs. TCP alone; +$P < 0.05$, vs. TCP plus 100 μg/mL rhCyr61. (B) Effect of exogenous rhCyr61 on responsiveness of BM-MSCs to BMP-2. BM-MSCs were cultured on

TCP, yECM or eECM in standard growth media; in addition, replicate cultures on TCP and eECM were also supplemented with 100 μg/mL rhCyr61. After 7 days of culture, cells were switched to low serum-containing media for 24 h, and then treated with BMP-2 (0.2 μg/mL) for 48 h. Runx2 expression was calculated relative to GAPDH and the data shown are the mean ± 95% confidence interval (CI) for $N = 3$ replicates. $*P < 0.05$, vs. untreated control. For each group, the fold-change with BMP-2 treatment versus untreated control is shown over each pair of bars. (C) Exogenous rhCyr61 (0–10 ng) does not incorporate into eECM after incubation for 24 h at 37C. yECM was used as a reference and at the end of incubation Cyr61 protein content in the eECM was assayed by Western blot.

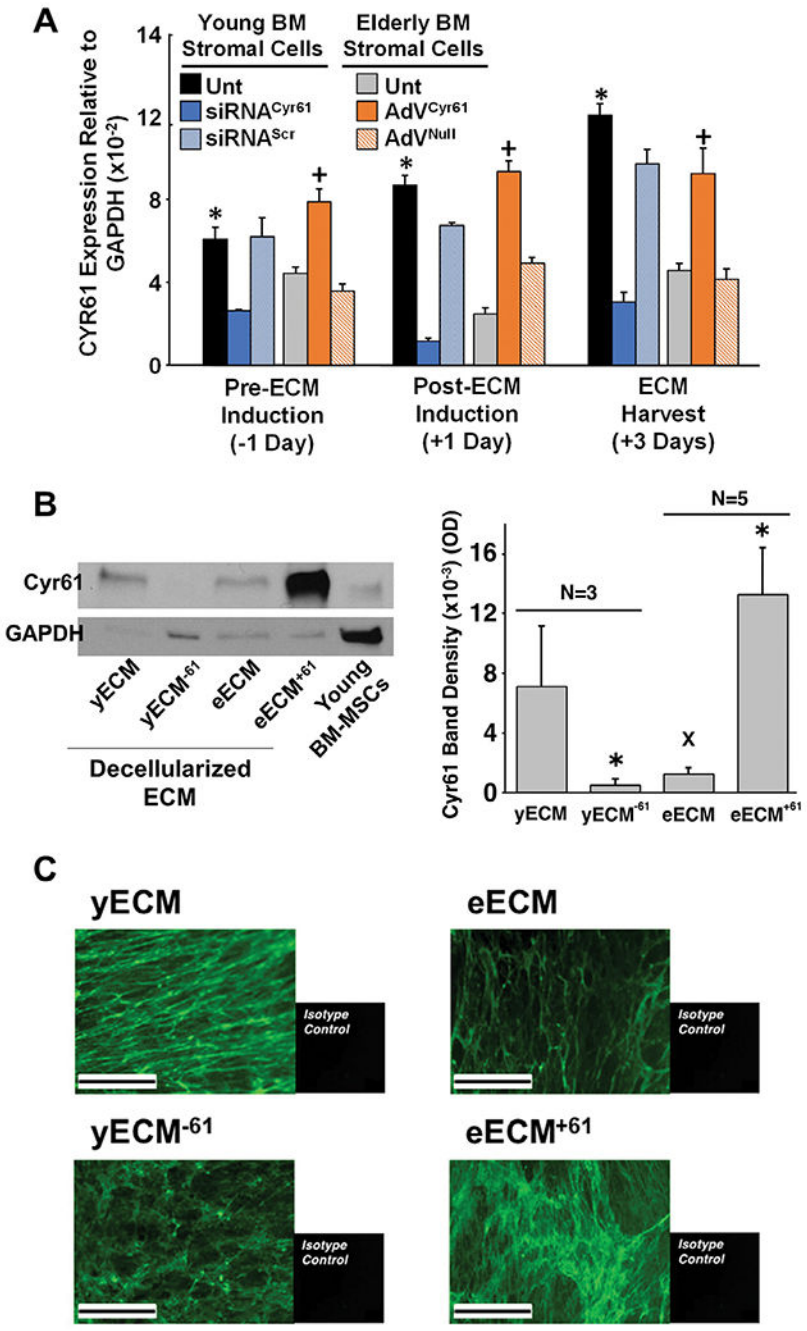

Fig. 6.

Incorporation of Cyr61 into the matrix can be manipulated by genetic modification of young and elderly BM stromal cells prior to ECM production. (A) Cyr61 expression during ECM synthesis is higher in young BM stromal cells relative to elderly, but treatment with siRNA or adenovirus, respectively, decreases or increases Cyr61 mRNA expression. Cyr61 expression was calculated relative to GAPDH and the data shown are the mean ± 95% confidence interval (CI) for $N = 3$ replicates. For each time point: $*P < 0.05$, vs. siRNA, untreated elderly, and adenovirus null; $+P < 0.05$, vs. untreated elderly, adenovirus null,

and siRNA. (B) Western blot analysis of yECM and eECM produced by BM stromal cells that were left untreated or genetically modified to decrease ($yECM^{-61}$) or increase ($eECM^{+61}$) the incorporation of Cyr61. (Left panel) Incorporation of Cyr61 protein was substantially reduced in yECM by treatment with siRNA ($yECM^{-61}$), while the adenoviral vector successfully enriched Cyr61 content in eECM ($eECM^{+61}$). To confirm the extent that the ECMs were decellularized, Cyr61 and GAPDH staining was performed on cell protein extracts of young BM-MSCs as a reference. (Right panel) Cyr61 Western blot band intensity for each ECM was quantified using optical density (OD) as in Fig. 4. The data are reported as the mean ± 95% confidence interval (CI) for $N = 3$ replicates for yECM and $yECM^{-61}$; $N = 5$ replicates for eECM and $eECM^{+61}$. $*P < 0.05$, vs. ECM not genetically modified; $\times P < 0.05$, vs. yECM. (C) Immunofluorescence staining of modified yECM and eECM shows modulation of Cyr61 incorporation by treatment with siRNA or adenovirus. ECM sections were prepared from cultures of young BM stromal cells (untreated, Cyr61-siRNA) and elderly BM stromal cells (untreated, Cyr61-adenoviral vector), stained for Cyr61, and immunofluorescence microscopy performed. Scale = 100 μm.

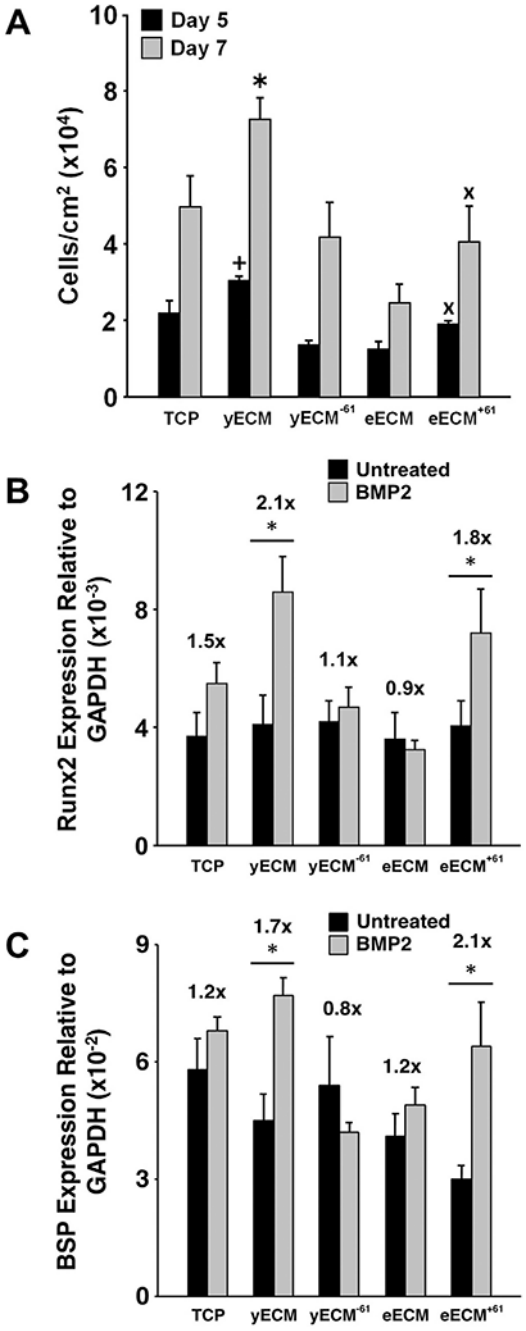

Fig. 7.

ECM-bound Cyr61 is an important regulator of BM-MSC function. (A) ECM-bound Cyr61 promotes BM-MSC proliferation. BM-MSCs were cultured for 5 or 7 days in standard growth media on TCP and untreated or genetically modified yECM and eECM to up- or down-regulate Cyr61 incorporation in the matrix. The data are presented as the number of cells/cm^2 and reported as the mean ± 95% confidence interval (CI) for $N = 3$ replicates. *$P < 0.05$, day 7 yECM vs. all other day 7 conditions; $^{+}P < 0.05$, day 5 yECM vs. all other day 5 treatment conditions; ^{x} $P < 0.05$, same day on eECM. (B-C) ECM-bound Cyr61 regulates

BM-MSC responsiveness to BMP-2. BM-MSC response to BMP-2 was reduced by culture on yECM^{-61}, relative to unmodified yECM. In contrast, BM-MSC response to growth factor treatment was restored by culture on eECM^{+61}, compared to unmodified eECM. Cultures on TCP and ECM produced by young, elderly, and genetically modified BM stromal cells were performed as described in Fig. 1; expression of Runx2 (B) and BSP (C) was measured after BMP-2 treatment (48-hours). Gene expression is calculated relative to GAPDH and the data shown are the mean ± 95% confidence interval (CI) for $N = 3$ replicates from three individual samples. *$P < 0.05$, vs. untreated control. For each group, the fold-change with BMP-2 treatment versus untreated control is shown over each pair of bars. *$P < 0.05$, vs. untreated control.

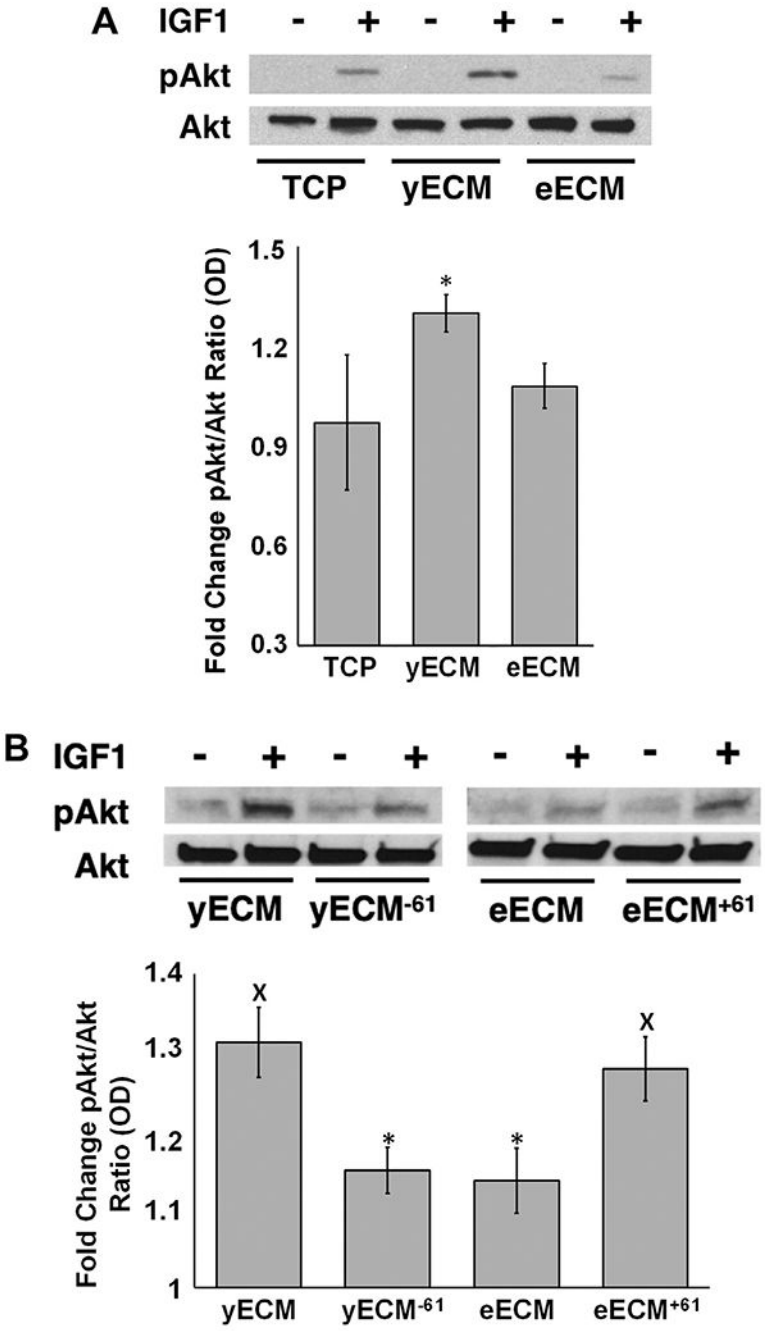

Fig. 8.

ECM-bound Cyr61 regulates BM-MSC responsiveness to IGF-1. (A) Culture on yECM increases the response of BM-MSCs to IGF-1 treatment relative to culture on eECM or TCP. (Top panel) Western blot analysis of pAkt and Akt expression by BM-MSCs cultured on TCP, yECM, or eECM and either treated or not treated with IGF-1. (Lower panel) Western blot band intensity for pAkt and Akt was quantified using ImageJ software and a pAkt/Akt ratio calculated. The data are reported as mean fold change in pAkt/Akt ratios ± 95% confidence interval (CI) for $N = 3$ replicates on TCP, yECM and eECM. *$P < 0.05$, vs. TCP.

(B) Depletion of Cyr61 reduces the ability of yECM to promote IGF-1 responsiveness, while increasing Cyr61 restores the capacity of eECM to promote growth factor responsiveness. (Top panel) Western blot analysis of pAkt and Akt expression by BM-MSCs cultured on Cyr61-modified yECM and eECM and either treated or not treated with IGF-1. (Lower panel) Western blot band intensity for pAkt and Akt was quantified with ImageJ (as above and in Fig. 4) and a pAkt/Akt ratio calculated. The data are reported as mean fold change in pAkt/Akt ratios ± 95% confidence interval (CI) for $N = 3$ replicates on yECM, yECM^{-61}, eECM, and eECM^{+61}. $*P < 0.05$, vs. yECM; $^{\times}P < 0.05$, vs. eECM.

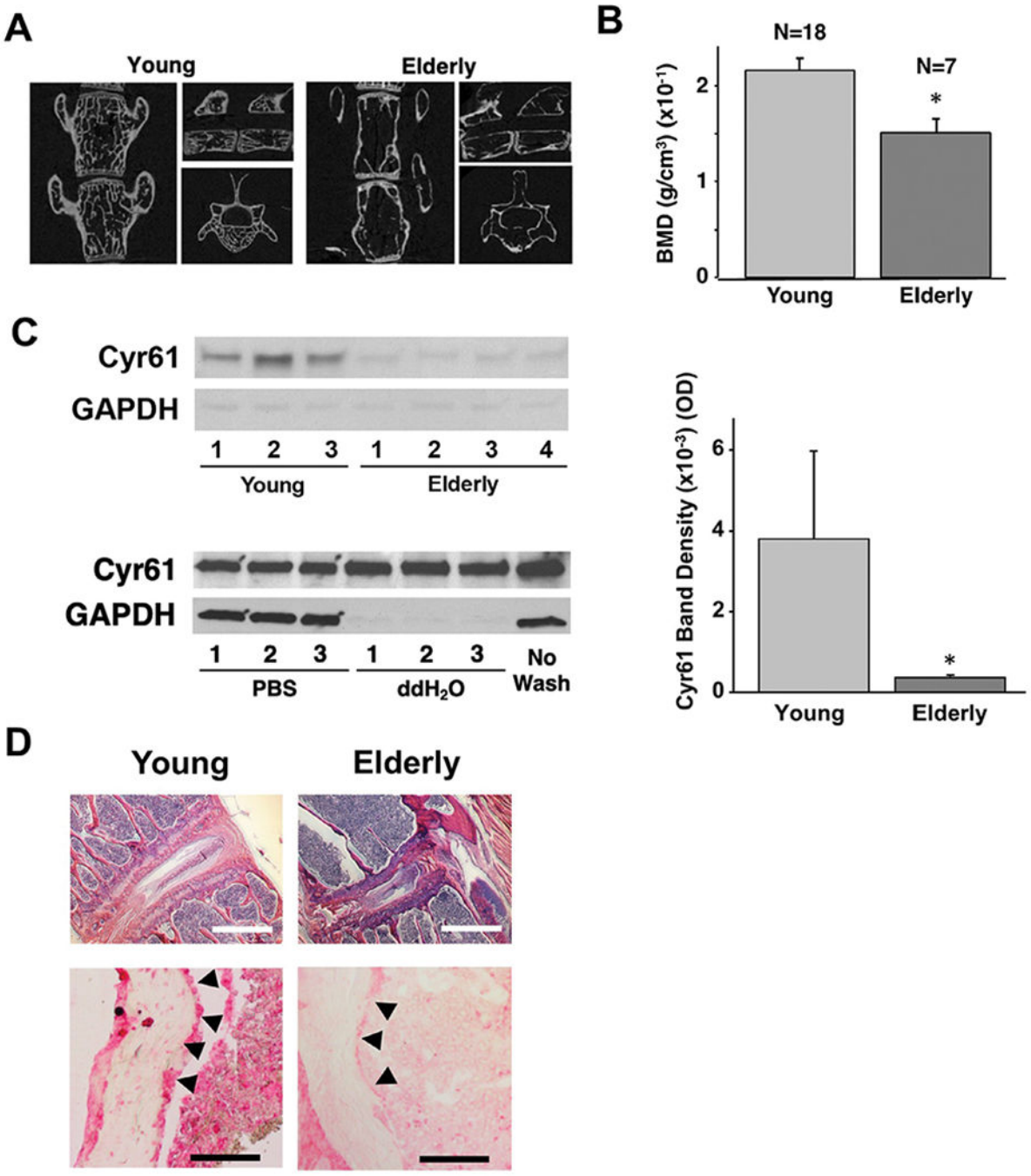

Fig. 9.

Vertebral bone mineral density declines with aging in mice. (A) Representative transverse, longitudinal, and radial cross-section μCT images of L4-L5 vertebrae from young and elderly mice. A well-defined loss of BMD in elderly mice can be seen. (B) Mean L4-L5 vertebral BMD measured in 18 individual young (9–11 months old) and 7 elderly (21 −23 months old) male and female mice. Error bars represent the 95% CI. *$P < 0.05$, vs. young. Statistical significance for elderly versus young vertebral BMD was confirmed with a two-tailed Student's T-test ($p = 4.19 \times 10–6$). (C) Western blot analysis of Cyr61 in extracts

of decellularized L4-L5 vertebral bone from young (<4 months old) and elderly (>21 months old) male and female mice. (Left panel) Extracts of young bone tissue contain a higher amount of Cyr61 protein relative to elderly. Staining for GAPDH was used to assess the success of the decellularization process using PBS vs. water. Water was ultimately chosen due to the completeness it provides in removing cellular constituents from the samples. (Right panel) Western blot band intensity of samples shown in the left panel were quantified as described in Figs. 4 and 6. Error bars represent the 95% CI. *$P < 0.05$, vs. young. (D) Representative histology of young and elderly L4-L5 vertebrae. (Top panel) H&E staining of young bone shows extensive trabeculae, which are substantially reduced in elderly bone. Scale = 500 μm. (Bottom panel) Immunostaining of Cyr61 in sections of young and elderly mice vertebrae.

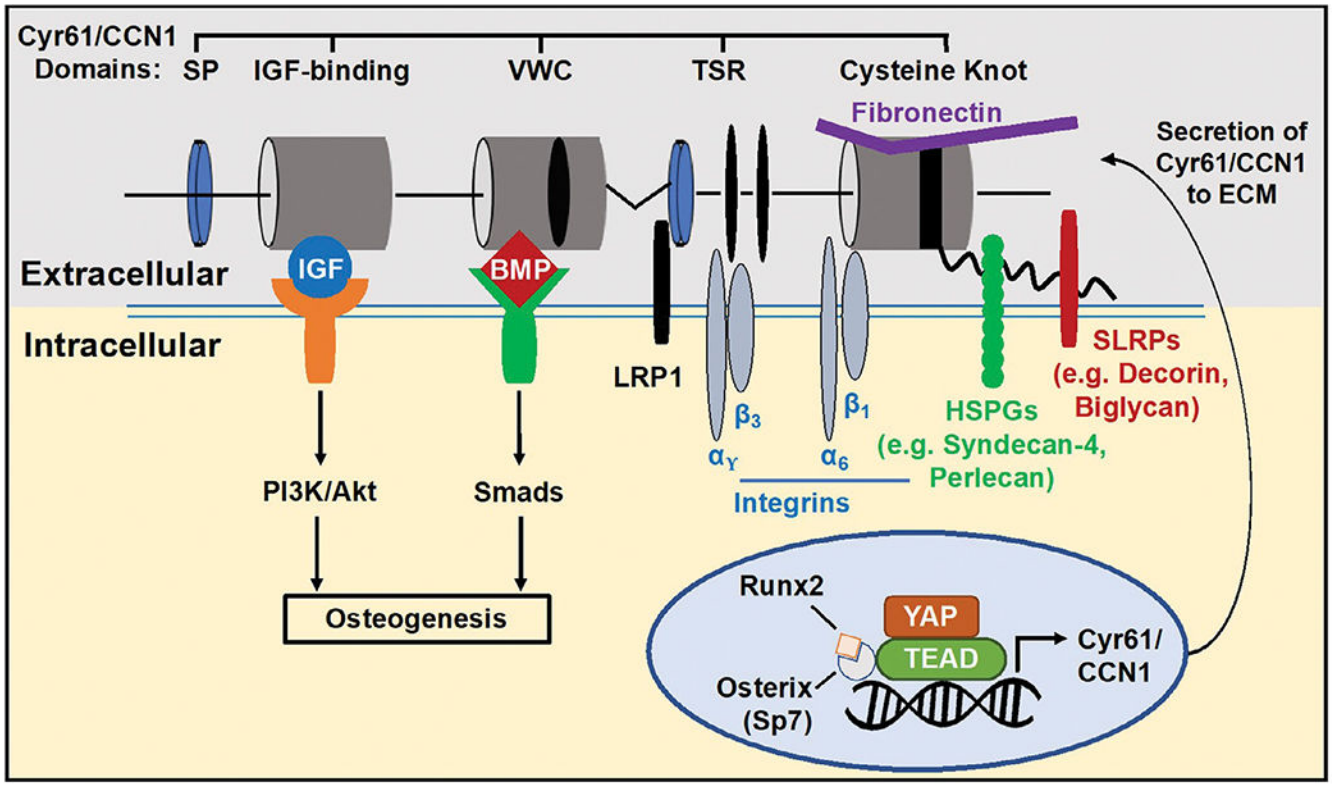

Fig. 10.

Proposed model illustrating the potential mechanisms where ECM-bound Cyr61 may be involved in regulating the properties of the BM niche and retention of the BM-MSC phenotype. Cyr61 multifunctional domains bind integrins (i.e. αvβ3, α6β1), receptors (e.g. LRP1) and various ECM constituents (i.e. fibronectin, proteoglycans) which may influence architectural and mechanical cues in the ECM. Based on data reported in the current studies, ECM-bound Cyr61 also participates in promoting the response of BM-MSCs to both BMP-2 and IGF-1, potentially acting as a co-receptor or extracellular reservoir. In young bone, extensive Cyr61 staining (pink color) is evident in the BM stroma and bone lining cells (arrowheads). Elderly bone shows reduced staining for Cyr61 at the interface of the stroma and bone lining cells (arrowheads). Scale = 200 μm.